

UCLA

UCLA Electronic Theses and Dissertations

Title

Spire: A Biochemical Dissection of Nucleation Activity

Permalink

<https://escholarship.org/uc/item/8mq6f64k>

Author

Rasson, Amy

Publication Date

2014

Peer reviewed|Thesis/dissertation

UNIVERSITY OF CALIFORNIA

Los Angeles

Spire: A Biochemical Dissection of Nucleation Activity

A dissertation submitted in partial satisfaction of the
requirements for the Doctor of Philosophy
in Biochemistry and Molecular Biology

by

Amy Rasson

2014

ABSTRACT OF THE DISSERTATION

Spire: A Biochemical Dissection of Nucleation Activity

By

Amy Rasson

Doctor of Philosophy in Biochemistry and Molecular Biology

University of California, Los Angeles, 2014

Professor Margot E. Quinlan, Chair

The actin cytoskeleton is essential for cellular functions such as cell motility, division, and establishment and maintenance of cell shape. Just as important as the actin cytoskeleton are the proteins that stimulate filament assembly called nucleators. There are three classes of nucleators: the Arp2/3 complex, the formins, and the recently discovered Wasp Homology-2 (WH2)-family of nucleators. All three nucleate different types of actin structures and employ unique nucleating mechanisms to do so. Of the three classes of nucleators, we know the least about the WH2-nucleators. What we do know is that WH2-nucleators use a mechanism involving tandem WH2 domains to initiate actin filament assembly. Although the WH2-nucleators share a common domain, the current literature suggests they nucleate using different mechanisms. Previous studies suggest that Spire, a WH2-nucleator unique to metazoans and essential for polarity in developing oocytes and embryos, nucleates filaments by forming a linear

nucleus or protofilament. Here we use a biochemical approach to further investigate the mechanism of nucleation and to identify how Spir differs from other non-nucleating, WH2-containing proteins such as N-Wasp. We investigated the biochemical features of Spir and N-Wasp WH2 domains interacting with actin under both steady state and kinetic conditions. Despite their short and similar sequences, all WH2 domains show distinct effects on the multiple phases of actin assembly. We found that the third WH2 domain in Spir, WH2C, is unique and specialized for nucleation in its sequence and interaction with both monomeric and filamentous actin. Work with tandem nucleating constructs revealed that the order of the WH2 domains in Spir influence nucleation activity and the ability to cooperatively bind actin.

The dissertation of Amy Rasson is approved.

Emil Reisler

James A. Wohlschlegel

Margot E. Quinlan, Committee Chair

University of California, Los Angeles

2014

TABLE OF CONTENTS

Section	Pages
List of Tables and Figures	vii
Acknowledgements	ix
Vita	xi
Chapter 1: <i>Introduction</i>	1
Figures	8
References	12
Chapter 2: <i>Filament Assembly by Spire: Key Residues and Concerted Actin Binding</i>	14
Manuscript Front Matter	15
Abstract	16
Highlights	17
Introduction	18
Results	21
Discussion	29
Methods	33
Appendix: Modeling steady state polymerization titrations	39
Supplementary Methods	42
Figures	44
References	55
Chapter 3: <i>Preliminary Data Further Characterizing Spir WH2C</i>	57
Results	58
Methods	62
Figures	63
References	72

Chapter 4: <i>Conclusion</i>	73
Figures	79
References	80
Appendix: <i>Ct-Spir Purification</i>	81
Introduction	82
Results	84
Methods	88
Figures	89
References	97

List of Tables and Figures

Figures	Pages
Figure 1.1: Schematic representation of actin nucleation.	8
Figure 1.2: Domain organization of Spir.	9
Figure 1.3: Binding mode of WH2 domains on actin.	10
Figure 1.4: Models of Spir and actin complexes.	11
Figure 2.1: Domain order and key residues affect nucleation.	44
Figure 2.2: WH2 domains synergistically bind monomeric actin.	45
Figure 2.3: Inhibition of spontaneous actin polymerization by WH2 domains does not correlate with actin binding affinity.	46
Figure 2.4: Effects of individual WH2 domains on actin nucleation.	47
Figure 2.5: Elongation rates of actin determined by TIRF microscopy.	48
Figure 2.6: Effect of individual WH2 domains on actin at steady state.	49
Figure 2.7: Effects of K_{db} and K_{dr} on steady state actin polymerization.	50
Table 2.1: Summary of results.	51
Figure 2.S1: Fluorescence anisotropy experiments of each WH2 domain construct.	52
Figure 2.S2: Homology model of Spir WH2C and actin co- crystal.	53
Table 2.S1: WH2 Constructs.	54
Figure 3.1: Spir C3 and actin co-crystals.	63
Figure 3.2: Electron density Fo-Fc map.	64
Figure 3.3: Mutations in the bridge region.	65
Figure 3.4: Two point mutations in the bridge of WH2C have a minimal affect on nucleation.	66

Figure 3.5: Mutating and elongating the bridge of WH2C changed its effect on actin polymerization.	67
Figure 3.6: Replacing the bridge of W_a with that from WH2C makes a stronger nucleator.	68
Table 3.1: Summary of different crystal conditions describing the screens, temperature, and constructs used.	69
Table 3.2: Summary describing the type of crystals observed from different screens and the results from testing their diffraction.	70
Figure 4.1: A model of Spir nucleation.	79
Figure A.1: Ct-Spir in inclusion bodies require denaturing methods for purification.	89
Figure A.2: No increased soluble Spir detected from altering expression conditions.	90
Figure A.3: Ct-Spir 520-991 over-expressed BL21 <i>E. Coli</i> competent cells are lysed in the buffers as described using varying pHs, and concentrations of both salts and detergents.	91
Figure A.4: SpirC3A purification using two different methods.	92
Figure A.5: Schematic showing the different constructs used for purification.	93
Figure A.6: Co-Purification of Spir 627-991 and KIND.	94
Figure A.7: Pull-down data with Spir and KIND are inconclusive.	95

Acknowledgements

I would first like to thank my advisor and committee chair, Dr. Margot E. Quinlan for allowing me to be a part of her laboratory and fostering my scientific and analytical skills through out my graduate career. This dissertation would not have been possible without her continuous guidance and support. I suspect that I will be the only graduate student to be trained by Dr. Quinlan herself and am very appreciative of this. She has been a fantastic mentor and always made sure she was available to provide, sometimes much needed, advice. Secondly, I would like to thank all my committee members Dr. Reisler, Dr. Clarke, Dr. Wohlschlegel, and Dr. Payne for their dedication and support through out my graduate work.

All current and previous Quinlan lab members have been instrumental to my success and happiness while at UCLA. They have provided me with mental and emotional support, laughter, and ridiculous amount of inside jokes. Where is the white van? A special thank you goes to current and past postdocs Dr. Christina Vizcarra and Dr. Justin Bois for always making time for my numerous scientific questions. Additionally, I would also like to thank all of the many Quinlan Lab babies, in particular Conrad Merkel for always reminding me about the important things in life.

I want to acknowledge all of my wonderful family and friends. My mom and dad have always been supportive in any way I've needed, and my Los Angeles relatives and Lorant Family made me feel at home in SoCal. Of course I need to acknowledge Jennifer and Ryan Samstag for being my source of stability. I've slept on their couch more times than I can count. You both have enhanced my life substantially. PBJBFF! I especially would like to acknowledge my amazing fiancé, Dr. Edward J. Miracco. I can honestly say that this dissertation would not have been possible without him. He has

provided me with truly unconditional love and support, not to mention plenty of scientific help. He is a wonderful person and amazes me everyday.

Lastly, I would like to thank most of my 20's. I may not have used you the way you wanted, but I wouldn't change a thing.

VITA

Education

B.S. Biochemistry and Molecular Biology June 2008
Department of Chemistry and Biochemistry
University of California, Santa Cruz

Research Experience

Graduate Research Associate 2009-2014
Dr. Margot E. Quinlan Laboratory
Department of Chemistry and Molecular Biochemistry
University of California, Los Angeles

Undergraduate Research Associate 2006 – 2008
Dr. Seth M. Rubin Laboratory
Department of Chemistry and Biochemistry
University of California, Santa Cruz

Laboratory Research Associate 2006 – 2008
Monoclonal Antibodies Department
Santa Cruz Biotechnology, Inc.

Research Associate Summer 2005
Dr. Mary K. Firestone Laboratory
Department of Environmental Science Policy and Management
University of California, Berkeley

Laboratory Research Intern Summer 2004
Dr. Jeffery A. Bird Laboratory
Lawrence Berkeley National Laboratory

Fellowships

Technology Transfer Fellow Summer, Fall 2013
Office of Intellectual Property
University of California, Los Angeles

Manuscripts & Posters

Rasson A, Bois J, Pham S, Quinlan M, *Filament Assembly by Spire: Key Residues and Concerted Actin Binding*. Manuscript submitted to the Journal of Molecular Biology, April 2014.

Rasson A, Pham S, Bois J, Quinlan M, *Mechanistic studies of a WH2-based actin nucleator, Spire*. Poster presented at the Seaborg Symposium, University of California, Los Angeles 2014

Rasson A, Pham S, Bois J, Quinlan M, *Mechanistic studies of a WH2-based actin nucleator, Spire*. Poster presented at the American Society for Cell Biology Annual Meeting, San Francisco 2012

Rasson A, Pham S, Bois J, Quinlan M, *Mechanistic studies of a WH2-based actin nucleator, Spire*. Poster presented at the Seaborg Symposium, University of California, Los Angeles 2011

Graduate Teaching Experience

Teaching Assistant,
University of California, Los Angeles
Department of Chemistry and Biochemistry

CHEM 156: Physical Biochemistry, Spring 2010
CHEM 154L: Biochemistry Laboratory, Winter, Spring 2009

Graduate Mentoring

Tsz Mei Cheung Fall 2012
Chemistry and Biochemistry graduate student, UCLA

Grant Shoffner Spring 2012
ACCESS, UCLA

Stephen Pham 2011-2012
Biophysics undergraduate student, UCLA

Volunteering

Science Buddies Expert, ScienceBuddies.org 2013

Chapter 1: Introduction

Actin Cytoskeleton

Actin is a 42-kDa globular protein and the most abundant protein in most eukaryotic cells. It forms the basic unit of the actin cytoskeleton, which plays a major role in many cellular processes. Actin monomers (G-actin) can polymerize into polar filaments (F-actin) that combine to form different structures involved in tasks such as producing a forward force for cell motility or tension for cell division (Figure 1.1 A). Generally actin filament polymerization occurs in three phases: nucleation, elongation, and steady state. During nucleation, three actin monomers form a stable complex in an energetically unfavorable event from which a filament can then elongate. During elongation, actin monomers rapidly add to the barbed, fast growing end, and in steady state, filaments reach a state where disassembly of monomers from the pointed, slow growing end is balanced by the amount of monomers adding to the barbed end—this steady state assembly and disassembly is known as ‘treadmilling’. The highly dynamic nature of actin polymerization is what allows it to play a critical role in cellular processes that require relatively rapid mechanical changes such as cell motility, cell division, and maintaining cellular shapes.

Actin Nucleators

The actin cytoskeleton is tightly regulated by a large number of actin binding proteins, each controlling different steps of assembly, including filament nucleation, elongation, depolymerization, capping, and severing. One class of actin binding proteins called nucleators, reduces the kinetic barriers of actin nucleus formation. They determine when, where, and influence what type of actin structures are formed. To date there are three known classes of actin nucleators (Figure 1.1 B). The Arp2/3 complex, the first nucleator discovered, binds the sides of pre-existing filaments to promote actin nucleation, creating branched actin structures specialized for producing force [1]. The

formin-family of nucleators form unbranched linear actin structures, which are best suited for creating tension; they stabilize a nucleus and processively ride along the barbed end of the filament, protecting it as it grows [2]. The third, most recently discovered and least studied class of actin nucleators are the WH2-nucleators. As their name implies they use multiple G-actin binding Wasp Homology-2 (WH2) domains to create a nucleus and stimulate actin filament polymerization [3]. Despite significant sequence variability, the individual WH2 domains display a similar overall fold and binding path on G-actin (Figure 1.3). An N-terminal amphipathic α -helix binds to actin in its hydrophobic cleft between actin subdomains 1 and 3. Following the helix is a conserved “LKKT/V” motif that extends along the outer surface of the actin monomer toward actin subdomain 2.

Very little is known about the mechanism by which any of the WH2-nucleators initiates actin assembly. The proteins Spir, JMY, Cordon bleu (Cobl), Leimodin (Lmod), and the bacterial proteins VopF/L/N are all part of the WH2-nucleator family and are thought to nucleate through distinct mechanisms [3-8]. Interestingly not all proteins containing multiple WH2-domains can nucleate actin filaments. In fact, they were originally identified in proteins that activate the Arp2/3 complex such as N-Wasp, which contains two WH2 domains. In addition to using multiple WH2 domains, WH2-nucleators need an extra motif or domain that links the WH2 domains together. In Spir this domain is named Linker 3 and connects the last two WH2 domains in the WH2 cluster [3, 6]. No structural data for this motif exists despite numerous attempts by multiple groups.

Unlike the well-studied Arp2/3 complex and formin nucleators, there is only one known actin structure made by WH2-nucleators—the actin mesh [9]. This structure is a poorly organized crosslinking of actin filaments much like the wool woven in a sweater. The actin mesh was first identified in the *Drosophila* oocyte and is essential to polarity and cell development [9, 10].

The Actin Mesh

During *Drosophila* oogenesis actin nucleators are critical to the establishment of anterior-posterior and dorsal-ventral axes. The oocyte develops in an egg chamber, which is made up of 16 germline cells. The remaining 15 cells become nurse cells, which support the developing oocyte. A major cytoskeletal rearrangement occurs during a later stage of oogenesis, stage 10b. At this time, the contents of the nurse cells are squeezed into the oocyte and a microtubule-dependent process, called cytoplasmic streaming begins [11-13]. If cytoplasmic streaming occurs prematurely, numerous deleterious effects are observed including polarity defects, female sterility, and birth defects [14, 15]. This demonstrates the temporal importance of cytoplasmic streaming, and thus the regulation of this process is critical to the development and polarity of the oocyte.

Genetic screens were performed to identify factors essential to the establishment of the major body axes. The genes *spire* (Spir) and *cappuccino* (Capu) were identified as disruptive to both the anterior-posterior and dorsal-ventral axes [14]. Spir is a WH2-nucleator and Capu belongs to the formin family of nucleators. In mutant Spir and Capu oocytes, premature cytoplasmic streaming occurs, leading to failure of axis determination [14, 15]. Their phenotypes are similar to those caused by agents, such as cytochalasinD, that disrupt the actin cytoskeleton, which is consistent with Spir and Capu being nucleators [9, 10]. Dahlgaard *et al.* discovered that an actin mesh spans the *Drosophila* oocyte up until stage 10b. This actin mesh disappears concomitant with the onset of streaming. In Spir and Capu null flies they found that the actin mesh was missing in all stages resulting in premature cytoplasmic streaming [9]. Based on these and other experiments, it is thought that Spir and Capu build the actin mesh and that the actin mesh is responsible for inhibiting streaming. This suggests that Spir and Capu help maintain oocyte polarity by regulating the timing of streaming by building and

maintaining the actin mesh. A similar actin structure has also been found in vertebrate oocytes and is absent in mouse oocytes in which both Spir1 and Spir2 are knocked-down by RNAi [16, 17].

Spir

The Spir-family of proteins have several conserved domains based on sequence homology (Figure 1.2). The kinase non-catalytic C-lobe domain (KIND), which has sequence similarity to the C-lobe of PAK kinases, lies at the N-terminal half of Spir [18]. Adjacent to the KIND domain are four actin binding WH2 domains, named A, B, C, and D, which make up the WH2 cluster. The WH2 cluster is responsible for forming the actin nucleus, which leads to actin filament initiation [3]. The C-terminal half of Spir consists of a rabphilin-3a like domain (also known as a 'Spir box') and a modified FYVE (mFYVE) domain [19, 20]. Typically FYVE domains are zinc fingers known to bind phosphatidylinositol 3-phosphate, a phospholipid found in cell membranes. When expressed in mammalian cells, Spir associates with several membrane structures [20]. Spir localization is disrupted in fibroblast cells when mutations are introduced in either the Spir box or mFYVE domains, emphasizing the importance of the C-terminus [20]. The last motif, known as DEJL, is located at the C-terminus and is a putative docking site for the c-Jun N-terminal Kinase (JNK). An interaction between Spir and JNK was identified in a yeast-two hybrid screen followed by confirmed phosphorylation of Spir by JNK [19].

Previous work provided insight into possible models for the nucleation activity of Spir. Quinlan *et al.* first observed an elongated WH2 cluster of Spir bound to four actin monomers by electron microscopy [3]. Combining this structural information with biochemical data led to a model in which each WH2 domain binds one actin monomer to create an elongated protofilament which acts as a template for monomer addition

(Figure 1.4 A). Bosch *et al.* subsequently found that the WH2 domains of human Spir 1 (hSpir1) can bind to actin in a cooperative manner forming a stable complex [21]. They proposed that this complex is not a nucleus but is in fact a sequestration structure (Figure 1.4 B). Crystal structures from Rebowksi, *et al.* suggests that constructs containing tandem WH2 domains, bound to actin are ill suited to form an actin filament; they observed that the actin monomers were rotated $\sim 60^\circ$ more than adjacent monomers in other unbound F-actin structures [22]. It is unclear how relevant this structure is to Spir since it does not include Linker 3 and the WH2 domains used are from N-Wasp, a non-nucleating protein. Ducka *et al.*, on the other hand were able to co-crystalize Spir and actin complexes. They determined that Spir WH2D binds to actin in a conformation similar to previously crystalized WH2 domains and actin complexes but important structural information regarding the other Spir WH2 domains were missing, for example, the linker regions were disordered [23]. Recently, data from Chen *et al.* suggest multiple Spir and actin complexes may form in solution, including both nucleating and sequestration complexes (Figure 1.4 A, B) [24]. Further insight is needed to understand how WH2-nucleators associate with actin monomers to initiate nucleation.

Overview of My Dissertation

Understanding how nucleators work can give us insight into the structures they build. The lack of data explaining the mechanism of WH2-nucleators and the significance of the actin mesh built by Spir motivated this research. My dissertation focuses on the WH2 domains of Spir to better understand mechanistically how WH2-based nucleators initiate polymerization of actin filaments and how they differ from those in non-nucleating WH2-containing proteins.

In chapter 2, we present our investigation of how WH2 domains from Spir and the WH2 domains from N-Wasp interact with monomeric and filamentous actin both on

their own and as tandem constructs. We performed equilibrium, steady state, and kinetic assays to understand how each WH2 domain contributes to the nucleation activity of Spir. We first created chimeras consisting of different pairs of WH2 domains connected by Linker 3 to identify how domain order affects nucleation activity. Strikingly, a construct with the WH2 domains reversed as compared to Spir had no nucleation activity. In addition, the position of Spir WH2C relative to Linker 3 had the largest influence on nucleation activity. We also found that, like hSpir1, our minimal nucleation construct of Spir binds to monomeric actin cooperatively [21]. Further, mutational analysis demonstrated that only two residues in WH2C were sufficient to convert a weak nucleator to the strength of Spir's wild-type activity. We also observed weak filament capping activities by Spir WH2A, and even more surprisingly, actin filament binding by WH2C. In sum, these studies highlight how different WH2 domains can be from one another and led to a model of how Spir nucleates.

In chapter 3, we present preliminary data further investigating the interesting results from Chapter 2 showing that Spir WH2C is specialized for nucleation. We attempted to determine the crystal structure of actin bound to WH2C to determine whether this WH2 domain differs from other previously solved actin/WH2 structures. We observed diffraction from a co-crystal of actin bound to a Spir construct containing WH2C and Linker 3 at a resolution of 3.7 Å but this resolution was not high enough to obtain useful side-chain information. We also initiated research on the region between the WH2 domain alpha helix and the conserved LKKV/T motif, which we refer to as the 'bridge region'. We modified the length and identity of the bridge region in WH2C of the minimal nucleation construct and found that we could create new interactions with actin that significantly affect nucleation activity [25].

Overall, my research contributes to the ongoing goal of understanding how Spir interacts with actin to nucleate filaments.

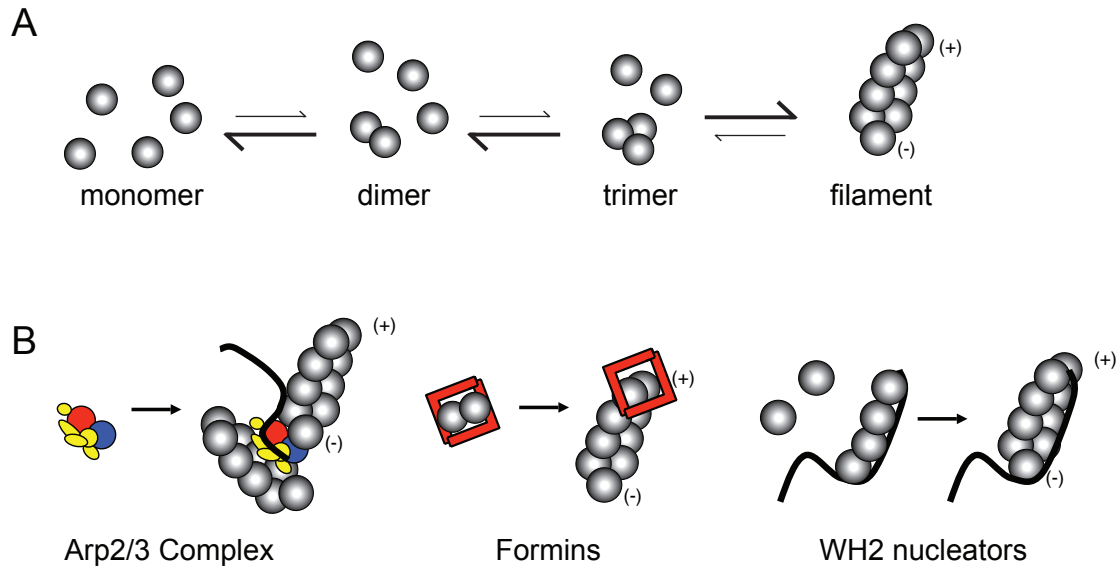


Figure 1.1: Schematic representation of actin nucleation. A. Spontaneous actin polymerization is energetically unfavorable, as represented by the thick and thin arrows. Once a trimer is formed addition of actin monomers proceeds quickly at the fast growing, barbed end (+) and slower at the slow growing, pointed end (-) of the filament. B. Three classes of nucleators – The Arp2/3 complex binds a pre-existing filament and provides a template for a second, branched filament. Formins stabilize a dimer to nucleate and then protect the fast growing end of that linear filament. WH2-nucleators bind multiple monomers, stabilizing a nucleus to build a new linear filament.

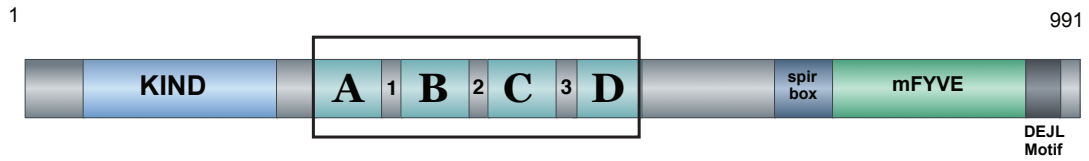


Figure 1.2: Domain organization of Spir. Spir isoform B is 991 amino acids in length: KIND is a kinase non-catalytic C-lobe domain; Four WH2 domains, depicted by the letters A, B, C, and D, are Wasp homology 2 actin monomer binding domains; Linker regions are depicted by the numbers 1, 2, and 3, which tether together the WH2 domains; SB – Spir box; mFYVE – modified FYVE domain. The black box contains the WH2 cluster, the site of Spir’s nucleation activity.

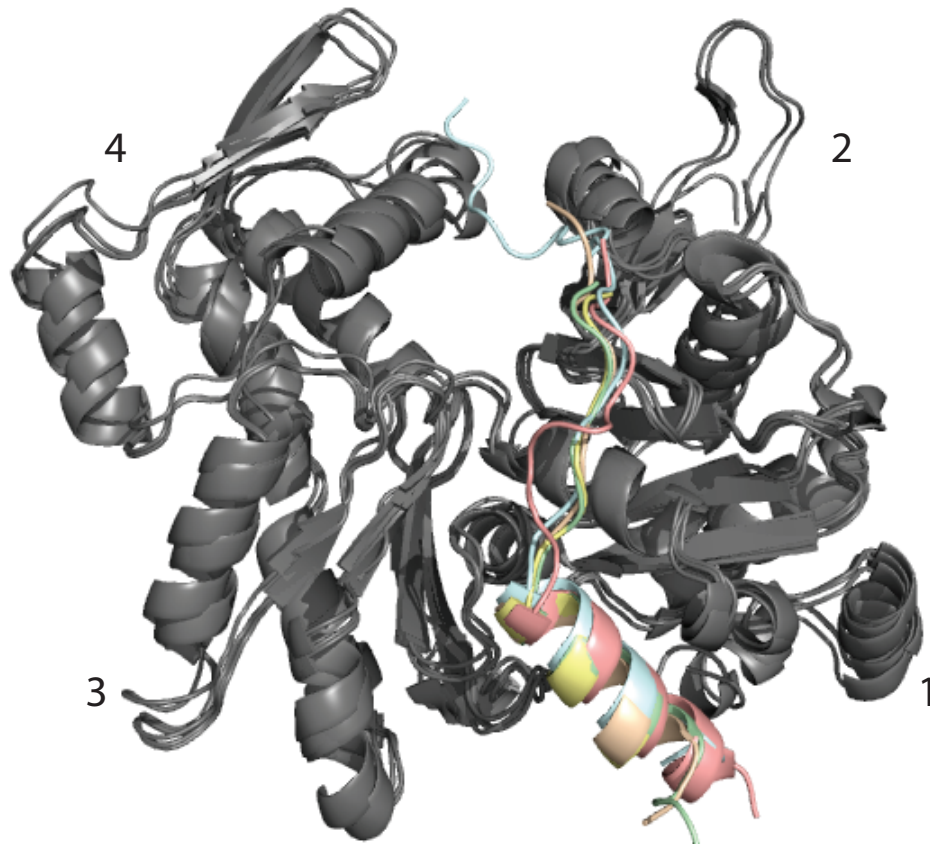


Figure 1.3: Binding mode of WH2 domains on actin. Alignment of actin (grey) and five WH2 domains (pastel) from various nucleating and non-nucleating proteins – dCiboulot first WH2 domain (PDB: 1SQK); hWasp (PDB: 2A3Z); hWAVE-2 first WH2 domain (PDB: 2A40); hWIP first WH2 domain (PDB: 2A41); and dSpir WH2D (PDB: 4EFH). Subdomains of actin are indicated by the numbers 1-4.

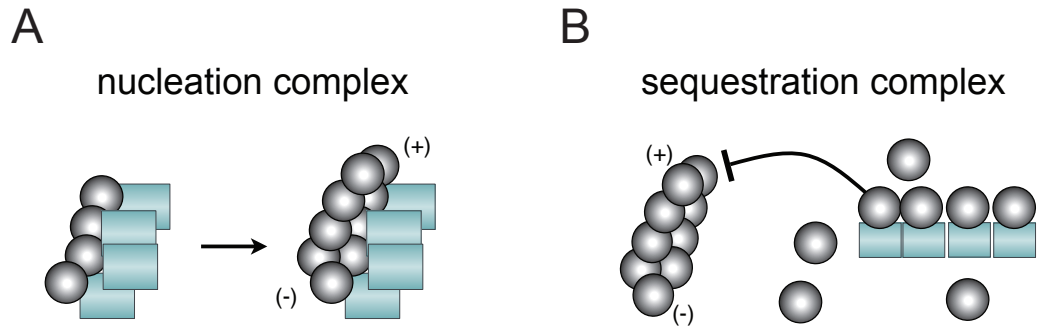


Figure 1.4: Models of Spir and actin complexes. A. Is the initially proposed model explaining how spire nucleates actin filaments. WH2 domains of Spir can bind to actin monomers forming a protofilament acting as a template for further monomer addition. B. An opposing model shows Spir WH2 domains forming a stable complex with four actin monomers that is unable to form a nucleus for actin polymerization. Teal squares are Spir WH2 domains and grey circles represent actin monomers.

References

- [1] Pollard, T.D. and G.G. Borisy Cellular motility driven by assembly and disassembly of actin filaments. *Cell* 2003;112:453-465.
- [2] Pring, M., M. Evangelista, C. Boone, C. Yang, and S.H. Zigmond Mechanism of formin-induced nucleation of actin filaments. *Biochemistry* 2003;42:486-496.
- [3] Quinlan, M.E., J.E. Heuser, E. Kerkhoff, and R.D. Mullins *Drosophila* Spire is an actin nucleation factor. *Nature* 2005;433:382-388.
- [4] Ahuja, R., et al. Cordon-bleu is an actin nucleation factor and controls neuronal morphology. *Cell* 2007;131:337-350.
- [5] Chereau, D., et al. Leiomodin is an actin filament nucleator in muscle cells. *Science* 2008;320:239-243.
- [6] Zuchero, J.B., A.S. Coutts, M.E. Quinlan, N.B. Thangue, and R.D. Mullins p53-cofactor JMY is a multifunctional actin nucleation factor. *Nat Cell Biol* 2009;11:451-459.
- [7] Liverman, A.D., et al. Arp2/3-independent assembly of actin by *Vibrio* type III effector VopL. *Proc Natl Acad Sci U S A* 2007;104:17117-17122.
- [8] Tam, V.C., D. Serruto, M. Dziejman, W. Brieher, and J.J. Mekalanos A type III secretion system in *Vibrio cholerae* translocates a formin/spire hybrid-like actin nucleator to promote intestinal colonization. *Cell Host Microbe* 2007;1:95-107.
- [9] Dahlgaard, K., A.A. Raposo, T. Niccoli, and D. St Johnston Capu and Spire assemble a cytoplasmic actin mesh that maintains microtubule organization in the *Drosophila* oocyte. *Dev Cell* 2007;13:539-553.
- [10] Emmons, S., H. Phan, J. Calley, W. Chen, B. James, and L. Manseau Cappuccino, a *Drosophila* maternal effect gene required for polarity of the egg and embryo, is related to the vertebrate limb deformity locus. *Genes Dev* 1995;9:2482-2494.
- [11] Theurkauf, W.E. Microtubules and cytoplasm organization during *Drosophila* oogenesis. *Dev Biol* 1994;165:352-360.
- [12] Palacios, I.M. and D. St Johnston Kinesin light chain-independent function of the Kinesin heavy chain in cytoplasmic streaming and posterior localisation in the *Drosophila* oocyte. *Development* 2002;129:5473-5485.
- [13] Serbus, L.R., B.J. Cha, W.E. Theurkauf, and W.M. Saxton Dynein and the actin cytoskeleton control kinesin-driven cytoplasmic streaming in *Drosophila* oocytes. *Development* 2005;132:3743-3752.
- [14] Manseau, L.J. and T. Schupbach cappuccino and spire: two unique maternal-effect loci required for both the anteroposterior and dorsoventral patterns of the *Drosophila* embryo. *Genes Dev* 1989;3:1437-1452.
- [15] Theurkauf, W.E. Premature microtubule-dependent cytoplasmic streaming in cappuccino and spire mutant oocytes. *Science* 1994;265:2093-2096.
- [16] Schuh, M. and J. Ellenberg A new model for asymmetric spindle positioning in mouse oocytes. *Curr Biol* 2008;18:1986-1992.
- [17] Pfender, S., V. Kuznetsov, S. Pleiser, E. Kerkhoff, and M. Schuh Spire-type actin nucleators cooperate with Formin-2 to drive asymmetric oocyte division. *Curr Biol* 2011;21:955-960.
- [18] Ciccarelli, F.D., P. Bork, and E. Kerkhoff The KIND module: a putative signalling domain evolved from the C lobe of the protein kinase fold. *Trends Biochem Sci* 2003;28:349-352.

- [19] Otto, I.M., T. Raabe, U.E. Rennefahrt, P. Bork, U.R. Rapp, and E. Kerkhoff The p150-Spir protein provides a link between c-Jun N-terminal kinase function and actin reorganization. *Curr Biol* 2000;10:345-348.
- [20] Kerkhoff, E., et al. The Spir actin organizers are involved in vesicle transport processes. *Curr Biol* 2001;11:1963-1968.
- [21] Bosch, M., K.H. Le, B. Bugyi, J.J. Correia, L. Renault, and M.F. Carlier Analysis of the function of Spire in actin assembly and its synergy with formin and profilin. *Mol Cell* 2007;28:555-568.
- [22] Rebowski, G., M. Boczkowska, D.B. Hayes, L. Guo, T.C. Irving, and R. Dominguez X-ray scattering study of actin polymerization nuclei assembled by tandem W domains. *Proc Natl Acad Sci U S A* 2008;105:10785-10790.
- [23] Ducka, A.M., et al. Structures of actin-bound Wiskott-Aldrich syndrome protein homology 2 (WH2) domains of Spire and the implication for filament nucleation. *Proc Natl Acad Sci U S A* 2010;107:11757-11762.
- [24] Chen, C.K., M.R. Sawaya, M.L. Phillips, E. Reisler, and M.E. Quinlan Multiple forms of Spire-actin complexes and their functional consequences. *J Biol Chem* 2012;287:10684-10692.
- [25] Didry, D., et al. How a single residue in individual beta-thymosin/WH2 domains controls their functions in actin assembly. *EMBO J* 2012;31:1000-1013.

Chapter 2: Filament Assembly by Spire: Key Residues and Concerted Actin Binding

Filament Assembly by Spire: Key Residues and Concerted Actin Binding

Amy Rasson¹, Justin S. Bois^{1,3}, Duy S. Pham¹, Margot E. Quinlan^{1,2}

¹Department of Chemistry and Biochemistry, University of California Los Angeles, 607 Charles E. Young Drive, Los Angeles, California 90095, USA.

²Molecular Biology Institute at UCLA, Paul D. Boyer Hall, 611 Charles E. Young Drive East, Box 951570, Los Angeles, California 90095-1570, USA.

³current address for J.S.B. Division of Biology and Biological Engineering, California Institute of Technology, MC 114-96, Pasadena, CA 91125

*Correspondence should be addressed to M.E.Q.: margot@chem.ucla.edu, office 310-206-8064, fax 310-206-5213

Key Words: WH2, nucleation, actin, cytoskeleton, Spir

Abstract

The most recently identified class of actin nucleators, Wasp Homology domain 2 (WH2)-nucleators, use tandem repeats of monomeric actin-binding WH2 domains to facilitate actin nucleation. WH2 domains are involved in a wide variety of actin regulatory activities. Structurally, they are expected to clash with interprotomer contacts within the actin filament. Thus, the discovery of their role in nucleation was surprising. Here we use *Drosophila* Spire as a model system to investigate both how tandem WH2 domains can nucleate actin and what differentiates nucleating WH2-containing proteins from their non-nucleating counterparts. We found that the third WH2 domain in Spire, WH2C, plays a unique role. This WH2 domain differs from the others in that it binds filaments. In the context of a short nucleation construct (containing only two WH2 domains), placement of WH2C in the N-terminal position was required for the most potent nucleation. We identified two residues within WH2C that are critical for its activity. Using this information we were able to transform a weak actin nucleator into a strong one. Lastly, we found that cooperative binding between the WH2 domains of Spire and monomeric actin also contributes to nucleation and the native organization of the WH2 domains with respect to each other is necessary for cooperativity.

Highlights

- Domain order plays a critical role in nucleation activity by Spir.
- Cooperative actin binding contributes to nucleation.
- Two residues in WH2C are necessary for strong nucleation and sufficient to convert a weak nucleator into a potent one.
- The WH2 domains of Spir interact with both actin monomers and filaments in distinct ways.

Introduction

Actin polymerization is a tightly regulated event, essential to countless fundamental cellular processes. It follows that formation of new filaments (nucleation) and subsequent growth (elongation), as well as disassembly of filaments, are carefully controlled. Many of the proteins that regulate these actin dynamics contain a short (~20 amino acids) actin-binding motif called the Wasp Homology domain 2 (WH2). WH2 domains are components of proteins that sequester actin monomers, promote filament elongation, sever filaments, activate nucleators and even nucleate on their own. How can such a short sequence do so many different things? It is easy to imagine that the WH2 domain itself is simply an actin-binding module and that sequences flanking the WH2 domain determine its role. No doubt this is part of the story, but the WH2 domains themselves are not all equivalent.

Do WH2 domains differ because they bind to actin in distinct orientations? A number of WH2 domains have been co-crystalized with actin [23, 24, 26-30]. Despite variability in the short sequence, they bind actin in nearly identical orientations. The core WH2 domain begins with a three-turn amphipathic α -helix that binds actin in the hydrophobic cleft between subdomains 1 and 3. A short linker follows the helix and the core ends with a "LKKT/V" motif, which binds the monomer in an extended conformation reaching towards subdomain 2 of actin. Notably, the sequence beyond the LKKT/V is usually missing in actin co-crystals, bringing into question the significance of the contribution of residues adjacent to the core WH2 domain.

Recent findings reinforce the idea that sequences adjacent to WH2 cores do not define their role and instead suggest that equilibrium binding affinities help specify the nature of their interactions with actin. Two proteins, Tb4 and Ciboulot, contain motifs closely related to WH2 domains, which are often referred to as T β 4 domains. The first T β 4-like domain in Ciboulot (CibD1) is a permissive actin binder, meaning that its

association with actin monomers does not potently inhibit filament elongation, while T β 4 sequesters actin monomers. It is commonly thought that sequestration by T β 4 depends on its N-terminal half binding the barbed face of the actin monomer, thereby blocking interactions with the pointed end of a filament, while the C-terminal half of T β 4 wraps around the actin monomer, blocking interactions with the barbed end of a filament. Didry et al. (2012) found that small changes within the N-terminal halves of T β 4 and CibD1 were sufficient to reverse their interactions with actin [25]. Specifically, replacing one residue within the CibD1 linker (between the α -helix and the LKKT/V) with the corresponding residue from T β 4 led to 5-fold tighter binding and converted CibD1 from a protein that permitted filament elongation to an actin monomer sequesterer. Likewise, substituting the complimentary residue from CibD1 in T β 4 decreased binding ~20-fold and converted this protein to a permissive binder. Thus, the region beyond the WH2 domain does not define CibD1 or T β 4 activity and binding affinity plays a major role in determining the activity of these domains.

Can affinities explain how proteins with multiple WH2 domains function? Many of the proteins that contain tandem repeats of WH2 domains can nucleate actin assembly. These so-called WH2-nucleators include several eukaryotic proteins, such as Cordon bleu (Cobl), JMY and Spire (Spir) [3, 4, 6, 31]. They are implicated in a variety of physiological processes including neural development and polarity establishment [14, 32-35]. The tandem WH2 construction has also been co-opted by some pathogenic bacteria, which use them to hijack the host actin cytoskeleton [7, 8]. WH2-nucleators are commonly considered a single class of actin nucleators although they function by distinct mechanisms. How their constituent WH2 domains define these mechanisms is not known.

Here we focus on Spir, a protein first described as a *Drosophila* polarity factor and since identified as essential to oogenesis in mammals as well as flies [14, 17]. Spir

has four tandem WH2 domains and a ~15 amino acid linker sequence (called Linker 3 (L3) or the MBL domain) between the last two WH2 domains, all of which contribute to nucleation activity [3, 6]. The last two WH2 domains of Spir, flanking Linker 3, are an effective minimal nucleation unit [3, 6]. Previously, we used this information to build a synthetic actin nucleator [6]. We started with the tandem WH2 domains of N-Wasp, which do not nucleate [6, 27]. When we inserted Linker 3 between them, this construct could indeed stimulate actin assembly. However, it was notably weaker than the analogous minimal nucleating unit derived from Spir, suggesting that the sequences of the WH2 domains play an important role in nucleation. Mutagenesis of each of Spir's WH2 domains in the context of the N-terminal half of Spir indicated that all four WH2 domains contribute to nucleation to differing degrees [3]. These experiments left open the question of how important positioning with respect to Linker 3 is to nucleation versus the importance of the specific sequence of a given WH2 domain. To eliminate this complexity, in this study we used the minimal nucleation unit within Spir (C3D; Figure 2.1A) and variations on this model. Together, our data indicate that WH2C is specialized for a role in nucleation but its affinity for actin does not by itself define its role. Instead, we found that WH2C associates with actin in a second mode, filament binding. We also identified key residues within WH2C that make it an effective actin nucleator. Finally, our data suggest that a combination of kinetics and cooperative interactions define the roles of Spir's WH2 domains in nucleation.

Results

Domain order and key residues determine the nucleation activity of Spir

To study the importance of domain order and the specific sequence of a given WH2 domain to nucleation, we used the simplified system of WH2-L3-WH2 constructs. We tested a permuted set of peptides containing the WH2C and WH2D domains of Spir and the two WH2 domains from the non-nucleating N-Wasp, which we refer to as W_a and W_b (Figure 2.1B). We tested each construct in a pyrene actin polymerization assay, using the time until half-maximum polymerization ($t_{1/2}$) as a metric to compare the nucleation activity between the constructs. This set of constructs displayed a broad range of nucleating activities ($t_{1/2}$ s from ~180 s to 570 s; Figure 2.1C). The native Spir domain order, C3D, to which we refer as wild type, was the most potent nucleator ($t_{1/2} = 180 \pm 20$ s). C3C was somewhat weaker (230 ± 40 s) and D3D was much weaker (400 ± 30 s), confirming that the specific sequence of the WH2 domains contributes to activity levels. Strikingly, when C and D were reversed (D3C), nucleation activity was abolished ($t_{1/2}$ indistinguishable from actin alone, 570 ± 30 s). That is, two domains that normally nucleate fail to do so when their positions with respect to Linker 3 are changed, demonstrating the importance of domain order to nucleation activity.

We also observed that the identity of the N-terminal WH2 domain was a major determinant of nucleation activity. The strongest nucleators were the constructs with WH2C in the first position, C3D, C3C, and C3 W_b . We note that the plateau of C3C was lower than the other constructs, suggesting that this construct sequesters actin more than others, an activity previously reported for Spir [3]. Likewise, the two constructs with W_a in the N-terminal position, W_a 3 W_b and W_a 3D, had equivalent activities. We tested two additional constructs that contained only one WH2 domain and Linker 3, C3 and 3D. These had no detectable activity (data not shown), confirming that two WH2 domains are necessary for nucleation.

Because of the contribution WH2C makes to nucleation activity, we examined the impact its sequence has on the nucleation activity of C3D. We found that the residues flanking the conserved isoleucine and arginine within the α -helix of WH2C differ from those found in most other WH2 domains (Figure 2.1B). These residues are usually charged, but in WH2C, of all known Spir sequences, they are phenylalanine and serine (Phe-438 and Ser-441 in *Drosophila* Spir). To test what impact these residues have on nucleation activity, we replaced the cognate residues in N-Wasp W_a , Gln-408 and Glu-411, with those from WH2C and then connected it to Linker 3 and WH2D (W_a [FS]3D). We used W_a 3D, with no mutations, for a baseline (Figure 2.1D). W_a 3D nucleates with a $t_{1/2}$ of 290 s, whereas W_a [FS]3D was as potent as C3D with a $t_{1/2}$ of 180 s. Next, we made the converse mutations in C3D, replacing Phe-438 with glutamine and Ser-441 with glutamate (C[QE]3D). This mutant lost activity, exhibiting a $t_{1/2}$ similar to W_a 3D ($t_{1/2}$ = 260 s) (Figure 2.1D). Intriguingly, neither single point mutant in W_a 3D showed an effect on nucleation activity (data not shown). Thus, we can dramatically alter the ability of a WH2 domain to nucleate by changing only two residues.

In summary, we found that the order of the WH2 domains influences nucleation activity. In particular, placing WH2C N-terminal to Linker 3 creates the strongest nucleator and two residues within its α -helix are sufficient to impart this strong activity.

Cooperative binding by tandem WH2 domains depends on domain order

In order to understand how these domains contribute to the larger nucleating complexes, we measured equilibrium binding between actin and each individual WH2 domain using competition fluorescence anisotropy (Figure 2.2A). We measured binding in the same buffer conditions used in our actin assembly assays, using latrunculin B bound actin (latB-actin) to prevent polymerization. We first measured the affinity of AlexaFluor488 labeled WH2D with Lys-Cys-Lys added to the C-terminus of the domain

for labeling (WH2D-KCK-AlexaFluor488). We then competed labeled WH2D off by titrating in the unlabeled WH2 domains. Despite their short and similar sequences, equilibrium dissociation constants of the Spir WH2 domains vary by an order of magnitude (K_d : 0.09 - 1.13 μM ; Figure 2.2A, Figure S2.1; Table 2.1). WH2B and WH2C bind most tightly to monomeric actin (K_d s \leq 0.21 μM) while WH2A and WH2D bind with higher equilibrium dissociation constants (K_d s \geq 0.62 μM). We also asked whether the addition of Linker 3 altered the affinity of WH2C or WH2D. In neither case was the change dramatic: the K_d of C3 was 0.11 μM , about twice as tight as that for WH2C alone (K_d (C) = 0.21 μM); in contrast, 3D is actually a little weaker than WH2D alone (K_d (3D) = 0.78 μM vs. K_d (WH2D) = 0.62 μM). In our previously published co-crystal of C3D with actin, we observed WH2D and part of Linker 3 bound to actin [24]. Linker 3 extends away from the actin monomer, suggesting that it would not contribute significantly to equilibrium binding, consistent with what we report here. Because it is C-terminal to the WH2 domain, we imagine that Linker 3 is more likely to contact the actin monomer bound to WH2C, and could thereby increase the affinity of this WH2 domain for actin, as we see here.

We also measured the affinity of actin for W_a and WH2C containing the mutations tested in the larger constructs, W_a [FS]3D and C[QE]3D, respectively (Figure 2.2A, Figure S2.1; Table 2.1). Surprisingly, the affinities of WH2C and WH2C[QE] were similar (K_d (WH2C) = 0.31 μM vs. K_d (WH2C[QE]) = 0.15 μM) despite the impact these mutations had on nucleation activity ($t_{1/2}$ = 200 s vs. 260 s). In contrast, when the reverse mutations were made in W_a , both K_d and the $t_{1/2}$ changed significantly (K_d (W_a) = 0.71 vs. K_d (W_a [FS]) > 30 μM and $t_{1/2}$ = 300 vs. 180 s). This result is even more intriguing given that W_a [FS]3D has wild type-like nucleation activity but 3D has no nucleation activity. It

follows that equilibrium binding of individual WH2 domains and actin is not predictive of nucleation activity.

Next we examined equilibrium binding of two larger constructs, C3D and D3C. Cooperative binding between tandem WH2 domains and actin was described for a construct of human Spir1 that contains all four WH2 domains [21]. It was proposed that the cooperative binding led to formation of a stable structure that sequesters actin as opposed to a nucleus. Subsequent work with *Drosophila* Spir indicated that both sequestration structures and nuclei exist in a mixture of actin and Spir [24]. To ask whether cooperative actin binding contributes to nucleation we performed competition fluorescence anisotropy assays using the C3D and D3C constructs – two constructs with the same domains but one nucleates while the other does not. Data were analyzed using a two-site binding model. We assumed that the first binding event was equivalent to actin binding to either individual WH2 domain. Then, we performed regression analysis leaving the value of the second binding event as a free parameter (see Methods). The results for C3D yielded dissociation constants of 10 nM and 30 nM for a second actin monomer binding to either WH2C or WH2D, respectively (Figure 2.2B, grey line, Table 2.1). These K_d values are much lower than the independently measured K_d values, suggesting that the C3D construct exhibits positive cooperative binding. We performed the same analysis on D3C, and found the most probable dissociation constant for binding a second actin monomer is essentially infinite, that is, no actin binding is detected (Figure 2.2B, black line). Therefore, the inverted WH2 order eliminates actin binding to a second site, and, it follows, formation of a nucleus. These data support our earlier results that domain order influences nucleation activity. They also suggest that the order leads to enhanced binding affinity and that cooperative binding does play a role in formation of a nucleus.

Effects of WH2 domains on actin assembly

Our binding data suggest that the four Spir WH2 domains interact distinctly with actin at equilibrium. We next asked whether this was also true in a more dynamic assay. We tested the effects that each individual WH2 domain has on actin polymerization, monitored with a bulk pyrene-actin assembly assay. We performed this assay by adding different concentrations of each WH2 domain (1.5 - 18 μM) to 4 μM actin and initiating polymerization by adding salts. We show 3 μM WH2 as a representative case (Figure 2.3). Examination of the kinetic traces reveals that the four Spir WH2 domains inhibit spontaneous polymerization to similar degrees, an unexpected result given the wide range of affinities for actin they exhibit (Figure 2.3A). Specifically, if these proteins were sequestering, 3 μM WH2A would leave ~ 2 μM free actin and 3 μM WH2B would leave ~ 1.2 μM free actin at equilibrium. Despite this predicted difference, actin assembly under these two conditions is almost indistinguishable. In order to quantify this observation, we compared the maximum rates of polymerization (Table 2.1). As our initial inspection suggested, these values did not correlate with affinity for actin (Figure 2.3D).

Next, we asked whether addition of Linker 3 to either WH2C or WH2D changed the behavior of the WH2 domains (Figure 2.3B). We see a slight increase in actin sequestration by C3, shown by the decrease in the plateau compared to WH2C, which is consistent with the measured K_d s. Surprisingly, 3D is a markedly weaker polymerization inhibitor than WH2D alone despite the small difference seen in their affinities for monomeric actin. Although the C3D-actin co-crystal reported by Chen *et al.*, does not show an interaction between WH2D and Linker 3, these data suggest Linker 3 could alter the kinetics of binding between WH2D and actin. We also examined the components of the mutant chimeras we used in the experiments described above (Figure 2.3C). Of these, we note that W_a and WH2C[QE], both components of weaker

nucleators, inhibit spontaneous polymerization to the greatest degree. In contrast, W_a [FS] and WH2C, both components of potent nucleators, have only minimal inhibitory effect. Together these data suggest that WH2 domains that are well tuned for nucleation do not individually prevent polymerization; that is, they may readily release actin monomers once incorporated in a filament and/or have binding kinetics that favor filament elongation over sequestration.

Because we found that larger constructs bind actin cooperatively, it may not be surprising that interactions between individual WH2 domains and actin aren't predictive of the maximum polymerization rate at $t_{1/2}$. While this metric provides a good general metric for efficacy of actin assembly, construction of filaments involves nucleation, elongation, and steady state polymerization. To better understand the consequences of adding WH2 domains to the bulk actin polymerization assay, we conducted a series of experiments to isolate each phase of actin assembly.

Nucleation: First we examined early time points of the bulk actin polymerization assay, when nucleation is the dominant activity. There was no clear correlation between the rate of these traces and actin binding affinity (Figure 2.4). Most of the WH2 domains inhibited nucleation to some degree, as expected. Interestingly, addition of WH2C or W_a [FS], the two WH2 domains in the N-terminal position of the most potent nucleation constructs, had essentially no inhibitory effect.

Elongation: We used Total Internal Reflection Fluorescence (TIRF) microscopy to investigate the effects the individual WH2 domains have on elongation of actin filaments. Labeled phalloidin-stabilized actin seeds and 0.8 μ M (15%) fluorescently labeled actin were used to measure the rates of elongation in the presence of the WH2 domains (Fig 2.5A,B; Table 2.1). We either pre-incubated WH2 domains with actin or mixed them immediately before addition to the slide under polymerizing conditions. While the differences are subtle, elongation rates were significantly higher when actin

was pre-incubated with WH2A, B, or C ($p < 0.01$), suggesting that these constructs cap filament barbed ends weakly (Figure 2.5B). Only WH2A slowed elongation significantly compared to actin alone in both cases ($p < 0.01$). Based on the affinity we measured, we predict that 0.7 μM actin would be available for elongation in the presence of 1 μM WH2A at equilibrium. Surprisingly, the elongation rate is 4-fold lower than actin alone. We interpret this as evidence that WH2A binds filament barbed ends, slowing filament growth even when presented with the monomer first. The other Spir-WH2 domains appear to allow elongation as opposed to capping or sequestering under these conditions. In all cases, K_d failed to correlate with the elongation rate (Fig 2.5C).

Steady state: Finally, we performed steady state polymerization titration (SSPT) assays, in which various concentrations of a given WH2 domain were added to pre-polymerized pyrene actin and total fluorescence was measured after the mixture had come to steady state (Figure 2.6). As expected, increasing concentrations of WH2 domains caused a steady decrease in polymer concentration until no remaining polymer could be detected. We note that after 72 hours of incubation with polymerized actin, WH2B, and to a lesser extent WH2D and C3, did not reach steady state. This is evident from the concavity of the titration curve before saturation. $W_a[\text{FS}]$ does not bind actin tightly enough to cause a significant drop in fluorescence at the tested concentrations; therefore, we do not consider this case or WH2B in our analysis.

To analyze the SSTEP data, we developed a model of steady state polymerization and actin binding by WH2 domains (see Appendix). We first plotted the predicted concentrations of actin as a function of WH2 concentration, assuming that the WH2 domains act solely by sequestering actin monomers (Figure 2.6, blue lines). To do so, we fixed the K_d to the value measured for each WH2 domain. We note that data from constructs containing WH2C, in particular, differed from the predicted curves. Therefore, in our theoretical treatment we also considered barbed-end binding and binding to the

filaments by WH2 domains. As described in the appendix, we are not sensitive to barbed end binding (Figure 2.7A). It follows that we cannot independently test whether WH2A binds the end of actin filaments with this steady state assay. The assay is sensitive to filament binding, as we demonstrate by varying the affinity between WH2 domains and the actin filament (K_{df}) while keeping the affinity for actin monomer constant (Figure 2.7B). As K_{df} decreases, the corner concentration moves to the right (increases) and the curve becomes less sharp. This phenomenon occurs because the ability of WH2 domains to bind filaments shifts the equilibrium away from sequestration of actin monomers by WH2 domains.

We tested whether the discrepancies between our model and experimental data were due to binding of the WH2 domains to filaments sides by performing a regression with K_d constrained to the value we measured and with K_{df} as a free parameter. The deviations are recovered as shown with red lines (Figure 2.6, red lines). For constructs containing WH2C, the resulting K_{df} values are less than or equal to 2 μM , weaker than their respective affinities for actin monomers but tight enough to be consequential (Table 2.1). For WH2A, WH2D and 3D the K_{df} values are greater than 10 μM and less likely to be physiologically relevant (Table 2.1).

In summary, equilibrium binding does not predict behavior of WH2 domains in nucleation, elongation or steady state assays. All four Spir-WH2 domains are permissive binders, with WH2A having the strongest capping activity. Finally, WH2C is distinct in that it binds filaments as well as monomers.

Discussion

WH2C is unique in its contribution to the nucleation activity of Spir

We set out to determine how the WH2 domains of Spir contribute to actin nucleation and how they differ from WH2 domains in non-nucleating proteins. Our data suggest that WH2C is specialized for nucleation. In the context of a minimal nucleation complex, WH2-L3-WH2, we found that the most potent nucleating activity depended on having WH2C N-terminal to Linker 3, as it is in Spir. Closer examination of WH2C's sequence led us to two residues—Phe-438 and Ser-441—that are unique to WH2C. Supporting our claim that these residues are important, introducing them into a weaker construct (W_a3D) was sufficient to increase the activity to C3D levels. When modeled in complex with an actin monomer based on the WH2D/actin co-crystal by Chen *et al.*, these two residues are found near the end of the three-turn α -helix in the hydrophobic cleft of actin (Fig S2.2). We speculate that the large, hydrophobic Phe-438 can stack with Phe-352 of actin with minimal rearrangements. The stacking would cause a shift in the α -helix of WH2C, which would be unimpeded by the small, uncharged Ser-441, allowing it to be embedded deeper within the actin hydrophobic cleft. The modulated interaction between WH2C and the actin hydrophobic cleft may alter the stability of the typical interaction. Alternatively, it could change the path the adjacent sequence would take when extending out of the cleft, thereby allowing a unique interaction to occur. To date, several WH2/actin co-crystals have been obtained and they are all very similar to one another [23, 24, 26-30]. They provide little insight into how this domain can function in such distinct ways. We, and others, have tried to co-crystallize WH2C with actin without success. In both cases, we were working with constructs that contained multiple WH2 domains. Ducka *et al.*, may not have seen actin bound to WH2C because of the incompatibility of fully occupied tandem WH2 domains in crystal structures as reported by Rebowksi *et al.* Our attempts were with C3D and we were surprised to recover a

crystal with WH2D occupied but not WH2C despite the fact that WH2C alone binds actin more tightly [24]. Hopefully, future work will produce this crystal.

Consistent with our speculation that WH2C's interaction is distinct from the other WH2 domains, it was the only one that exhibited significant filament binding activity. While we do not know if this alternate binding is physiological, the affinity we measured, $\leq 2 \mu\text{M}$, suggests that it may be. The fact that this binding is approximately 10-fold weaker than for actin monomers indicates that more "traditional" monomer binding still dominates. However, because WH2 binding to the hydrophobic cleft of actin monomers is thought to be incompatible with longitudinal actin filament contacts [27, 36], an alternate interaction between WH2C and actin could contribute to nucleation activity, by allowing this region to "get out of the way" of the newly forming filament or perhaps by stabilizing the nucleus.

Previously, we carried out nucleation studies using the N-terminal half of Spir (SpirNT), which included the entire cluster of four WH2 domains [3]. Mutations to remove actin binding were introduced into each WH2 domain, one at a time. Mutating WH2D had the strongest effect, followed by mutations in WH2C. In contrast with our findings, these data suggested that WH2D contributes the most to nucleation. We believe the difference in observations depends on the construct. That is, two functioning WH2 domains must flank Linker 3 to form a functional nucleator. In the context of SpirNT, Linker 3 still has functional WH2 domains on either side of it when WH2C is mutated but not when WH2D is mutated. Thus the minimal nucleation construct was instrumental in revealing the important role of WH2C.

Spir has emergent properties

We found little to no correlation between affinity and how a WH2 domain affects actin assembly. This intriguing lack of correspondence was emphasized after studying

each of the three phases of actin polymerization in isolation—nucleation, elongation, and steady state. For example, Spir's four WH2 domains behaved similarly in bulk actin assembly assays despite affinities for actin that range over an order of magnitude. In addition, single filament elongation assays indicate that WH2A has some end capping activity and SSPT assays suggest that WH2C binds to the sides of filaments. These data show that interaction with actin of different WH2 domains can differ greatly and that Spir's nucleation activity cannot be predicted by the sum of its parts. Of course, actin assembly is a dynamic process and detailed kinetics assays as opposed to thermodynamics may be more useful for predictions.

However, we also observed that domain order is a significant determinant of nucleation activity: C3D is a strong nucleator, while the reversed construct, D3C, has no detectable nucleation activity. Here binding assays were able to provide insight. C3D bound actin in an apparently cooperative manner. This fits with the report of cooperative binding by a larger Spir construct [21]. We note that the effect required the presence of two WH2 domains, since adding Linker 3 to either WH2C or WH2D alone produced minimal changes in actin binding. We were intrigued to find that D3C binds actin in an anti-cooperative manner so extreme as to only support binding to a single actin monomer, despite the presence of two WH2 domains. This binding behavior explains why D3C fails to nucleate and emphasizes that Spir activity is greater than the sum of its parts.

How does Spir work?

Experimental data demonstrate that all four WH2 domains can bind actin but none works as a tight sequesterer, like T β 4. Comparison of our experimental observations to a theoretical framework revealed that WH2C also interacts with actin filaments. Given the evidence that Linker 3 plays an important role in nucleation, it is

perhaps fitting that WH2C, one of the domains adjacent to Linker 3, has an alternate binding modality. Our results also suggest that an ability to release actin is important for nucleation by these actin-binding motifs. Together these data support a model where each WH2 domain binds an actin monomer, brings them into close proximity with one another, and then subsequently adjusts without completely dissociating to allow for filament formation. Our data and that of Bosch et al., suggests that at least two structures can be formed – a nucleus and a stable sequestration complex. Future work will address when/how one or the other is built and what happens when Spir is dimerized, which accelerates nucleation, as is the case when it binds to Cappuccino [37, 38].

Methods

DNA constructs

Drosophila Spir and *R. rattus* N-Wasp constructs were generated by PCR amplification from full-length templates, CG10076 and D88461.1, respectively. Truncations were subcloned into the pGEX-6P-2 vector (GE Healthcare, Piscataway NJ) or pET20b(+) (Novagen, Hornsby Australia). Constructs used are depicted in Table S2.1. Point mutations were introduced using QuikChange Site Directed Mutagenesis (Stratagene, Santa Clara, CA). Chimeras were constructed by SOEing [39].

Protein purification and labeling

A. castellani actin was purified and labeled according to published protocols [38, 40]. WH2 containing constructs were expressed in *E. coli* BL21(DE3) cells and purified by standard protocols as described in Supplemental Methods. Briefly, proteins were purified on glutathione-Sepharose 4b. The GST-tag was removed with PreScission protease and a second exposure to glutathione resin. Single WH2-containing proteins were further purified by filtering over an anion exchange column (MonoQ, GE Healthcare) and collecting the flow through. The multiple WH2-containing constructs were purified on a cation exchange column (MonoS, GE Life Sciences). The final products were dialyzed against 10 mM Tris pH 8, and 1 mM DTT overnight at 4°C. Protein aliquots were flash-frozen in liquid nitrogen and stored at -80°C. Protein concentrations were calculated by quantitative SYPRO Red (Life Technologies, Grand Island, NY) stained gels using Amino Acid Analyzed (UCLA Biopolymer Laboratory) WH2D as a standard, due to their lack of absorbance at 280nm.

For actin assembly assays, actin was labeled with pyrene iodoacetamide as described [41]. For TIRF assays, actin was labeled with Oregon Green 488 iodoacetamide (Life Technologies, Carlsbad, CA) on cysteine-374 as described [42].

For anisotropy experiments, unlabeled WH2D-KCK was incubated for 20 min at 42 °C with 2 mM TCEP and then dialyzed twice for 2 h each against 10mM HEPES pH 7, 50 mM KCl. Protein was then rocked at 25 °C for 30 min with a 2-4 molar excess of AlexaFluor488-C5-maleimide. The reaction was quenched by addition of 10 mM DTT. Unconjugated dye was removed using a PD-10 desalting column (GE Life Sciences) equilibrated with 10 mM Tris-HCl pH 8.0, 1 mM DTT, 100 mM KCl. Protein concentration was determined by quantitative SYPRO Red staining. The concentration of incorporated dye was determined by absorbance at 496 nm using an extinction coefficient of 71,000 cm^{-1} . Labeling efficiency was calculated to be 58%.

Pyrene-actin polymerization assays

Pyrene-actin assembly assays were carried out essentially as described [43]. Briefly, 4 μM actin (5% pyrene labeled) was incubated for 2 min at 25°C with ME buffer (final concentration, 200 μM ethylene glycol tetraacetic acid [EGTA] and 50 μM MgCl_2) to convert Ca-G-actin to Mg-G-actin. Polymerization was initiated by adding KMEH polymerization buffer (final concentration, 10 mM HEPES, pH 7.0, 1 mM EGTA, 50 mM KCl, 1 mM MgCl_2) to the Mg-G-actin. WH2-containing proteins, were combined in the polymerization buffer before addition to Mg-G-actin. Fluorescence was monitored in a TECAN F200 (Tecan Group Ltd., Männedorf, Switzerland) with $\lambda_{\text{excitation}} = 365 \text{ nm}$ and $\lambda_{\text{emission}} = 407 \text{ nm}$. For pre-incubation experiments WH2-containing proteins were mixed with actin for 72 h at 4°C and warmed to room temperature for 30 minutes before addition of ME and KMEH.

Steady state polymerization titration

To test most of the WH2 domains, 2 μM actin (10% pyrene labeled) was polymerized in KMEH plus 0.5 mM Thesit for 1 h in a 96-well plate at 25°C. Single WH2-

containing proteins were titrated in and stored for 72 h at 4°C. The plate was allowed to warm to room temperature for 30 min before fluorescence was measured in a TECAN F200. For WH2A, the same procedure was followed except we used 0.5 μ M actin (40% labeled).

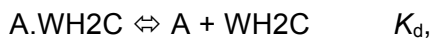
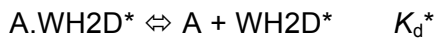
The SSPT curves were fit with the model described in the appendix with K_{db} set to infinite. The dissociation constants, K_{da} , for addition of an actin monomer to the end of a filament were determined from a critical concentration assays with 10% and 40% pyrene labeled actin (data not shown). The dissociation constants, K_d , for respective WH2 domains with actin monomers were constrained to the values determined from our competition anisotropy assays. The background pyrene fluorescence, p_{bg} was given by the mean of the last four points of the SSPT curve. For the blue curves, K_{df} was set to infinite, so p_{\sim} (a scaling factor) was the only free parameter in the regression. For the red curves, K_{df} was also a free parameter.

Polarization anisotropy

All assays were carried out with latrunculin bound actin (latB-actin) in 10 mM HEPES, pH 7.0, 1 mM EGTA, 1 mM TCEP, 0.5 mM Thesit, 50 mM KCl, and 1 mM $MgCl_2$ at 25°C. latB-actin was made by mixing a 2-fold molar excess of latB with actin for 1 h at 25°C.

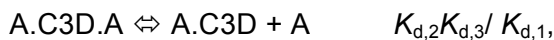
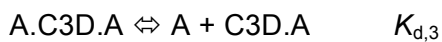
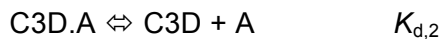
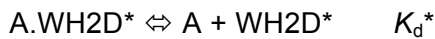
Fluorescence polarization anisotropy of 5 nM WH2D-KCK–AlexaFluor488 (58% labeled) mixed with 2 μ M latB-actin was measured with increasing concentrations of actin. The fluorophore was excited by plane-polarized light at 488 nm, and emission was measured at 520 nm at angles parallel and perpendicular to the angle of incidence using a TECAN F200 (Tecan Group Ltd., Männedorf, Switzerland). We performed a regression to determine the equilibrium dissociation constant, K_d^* , using a quadratic binding model as previously described [43].

Next, we added increasing amounts of competing individual WH2 domains to 5 nM WH2D-KCK-AlexaFluor488 and 2.0 μ M latB-actin. Given the previously measured value of K_d^* , the dissociation constants of the respective constructs were obtained using regression tools in EQTK (eqtk.org), a forthcoming analysis tool for coupled equilibria using algorithms from [44, 45]. Specifically, we performed a regression corresponding to the reactions, for example for WH2C,



where A is latB-actin and WH2D* is WH2D-KCK-AlexaFluor488, with similar analysis for WH2A, WH2B, WH2D, C3, 3D, W_a, WH2C[FS] and W_a[QE].

To investigate cooperative binding of actin by C3D, the reactions and dissociation constants considered in the regression analysis using EQTK were



where the dissociation constant for the last reaction is determined by the previous three as required by the path independence of equilibrium. An analogous set of reactions was used for D3C.

TIRF microscopy assays

Coverslips for TIRF elongation assays were prepared as described [24]. Briefly, they were silanized with 5% 3-aminopropyl-triethoxysilane (Sigma-Aldrich, St. Louis, MO) and PEGylated with N-hydroxysuccinimide-functionalized polyethylene glycol

(PEG-NHS; 97% methoxy-PEG-NHS and 3% biotin-PEG-NHS (JenKem Technology, Allen, TX).

Actin was biotinylated using maleimide-PEG11-biotin (Thermo Scientific, Waltham, MA) and mixed with AlexaFluor488-phalloidin at a 1:1 ratio to create 5% biotinylated phalloidin-stabilized actin seeds. Immediately before imaging, a blocking solution (PBS, 1% Pluronic, 0.1 mg/ml casein) was applied to the flow cells for 2 minutes followed by a wash with 1× TIRF buffer (50 mM KCl, 1 mM MgCl₂, 1 mM EGTA, 10 mM HEPES, pH 7, 0.2 mM ATP, 50 mM DTT, 0.4% methylcellulose). Next 40 nM streptavidin (VWR, Radnor, PA) was applied to the flow cell for 1 min, followed by a wash with 1× TIRF buffer, 30 s of incubation with 10-30 nM actin seeds, and a wash with 1× TIRF buffer. OG-actin (0.8 μM, 15%-OG-labeled final concentration) was incubated with ME buffer for 2 min at room temperature. A solution containing 2× TIRF buffer, glucose oxidase (final concentration 0.25 mg/ml), catalase (final concentration 0.05 mg/ml), and any test proteins (1 μM single WH2-containing proteins final concentration) was mixed with the Mg-G-actin solution and added to the flow cell. Filament elongation was visualized on a DMI6000 TIRF microscope (Leica, Wetzlar, Germany) for at least 20 min, capturing images at 10 s intervals. Filament lengths and elongation rates were analyzed with JFilament [46] incorporated into Fiji [47].

Spir WH2C model

Using SWISS-MODEL, the sequence of WH2C (residues 421 through 428 of *Drosophila melanogaster* SpireB) was threaded through the WH2D crystal structure bound to *A. castellanii* actin (PDB ID: 4EFH) [24, 48]. WH2D was then removed from 4EFH, replaced by the generated WH2C model, and the co-crystal model was visualized using UCSF Chimera [49].

Appendix: Modeling steady state polymerization titrations

To enable analysis of SSPT experiments, we derive here an expression for pyrene fluorescence intensity as a function of the concentration of a titrated WH2 domain. We successively use the law of mass action, combined with mass conservation of the total amount of actin monomer and WH2 molecules in the reaction vessel. The chemical reactions describing actin nucleation are based on Sept and McCammon [36]. In particular, we define the reactions involved in polymerization as



where A_n denotes an actin filament consisting of n monomers. The reactions have dissociation constant K_n with $K_n \equiv K_{\text{da}}$ for $n \geq 4$. The values of the first three equilibrium constants, which describe spontaneous nucleation, are immaterial, provided they are much smaller than K_{da} . We allow a WH2 domain to bind an actin monomer with dissociation constant K_{d} . In the most general case we also allow a WH2 domain to bind an actin monomer that is in a filament with dissociation constant K_{df} . We treat binding of a WH2 domain to the barbed end of a filament as a special case of filament binding with dissociation constant K_{db} .

Let c_{w} be the concentration of an unbound WH2 domain and c_{aw} be the concentration of a WH2 domain bound to monomeric actin. For a filament of length n with m bound WH2 domains with the barbed end unbound, there are $\binom{n-1}{m}$ ways to arrange the bound WH2 domains. If the barbed end is bound, there are $\frac{m}{n} \binom{n}{m}$ ways to arrange the bound domains. Let $c_{n,m,i}^u$ be the concentration of a *particular* arrangement i of WH2 domains on a filament with the barbed end unbound. Assuming the free energies of all arrangements for a given n and m are equal, so are their steady state concentrations; $c_{n,m,1}^u = c_{n,m,2}^u = \dots$. For notational convenience, we define this concentration to be $c_{n,m,i}^u \equiv c_{n,m}^u$. The concentration of filaments with barbed ends bound with WH2 are similarly defined with concentration $c_{n,m}^b$. The total concentration of filaments of length n with m bound WH2 domains is

$$\sum_i (c_{n,m,i}^u + c_{n,m,i}^b) = \binom{n-1}{m} c_{n,m}^u + \frac{m}{n} \binom{n}{m} c_{n,m}^b. \quad (2)$$

We can therefore write down expressions for conservation of total mass of actin and WH2.

$$c_a^0 = c_a + c_{aw} + 2(c_{2,0}^u + 2c_{2,1}^u + c_{2,2}^u) + 3(c_{3,0}^u + 3c_{3,1}^u + 3c_{3,2}^u + c_{3,3}^u) \\ + \sum_{n=4}^{\infty} \sum_{m=0}^{n-1} n \binom{n-1}{m} c_{n,m}^u + \sum_{n=4}^{\infty} \sum_{m=1}^n m \binom{n}{m} c_{n,m}^b \quad (3)$$

$$c_w^0 = c_w + c_{aw} + 2(c_{2,1}^u + c_{2,2}^u) + 3(c_{3,1}^u + 2c_{3,2}^u + c_{3,3}^u) \\ + \sum_{n=4}^{\infty} \sum_{m=1}^{n-1} m \binom{n-1}{m} c_{n,m}^u + \sum_{n=4}^{\infty} \sum_{m=1}^n \frac{m^2}{n} \binom{n}{m} c_{n,m}^b. \quad (4)$$

Using the law of mass action, we can write down the equilibrium concentrations of all non-monomeric species.

$$c_{aw} = \frac{c_a c_w}{K_d} \quad (5)$$

$$c_{2,m}^u = \frac{K_2}{K_{df}^m} c_a^2 c_w^m, \quad m = 0, 1, 2 \quad (6)$$

$$c_{3,m}^u = \frac{K_3}{K_{df}^m} c_a^3 c_w^m, \quad m = 0, 1, 2, 3 \quad (7)$$

$$c_{n,m}^u = K_4 K_{da}^4 \left(\frac{c_a}{K_{da}} \right)^n \left(\frac{c_w}{K_{df}} \right)^m, \quad n \geq 4, 0 \leq m \leq n-1 \quad (8)$$

$$c_{n,m}^b = \begin{cases} 0, & n < 4 \\ K_4 K_{da}^4 \left(\frac{c_a}{K_{da}} \right)^n \frac{c_w^m}{K_{df}^{m-1} K_{db}}, & n \geq 4, 1 \leq m \leq n. \end{cases} \quad (9)$$

Inserting these expressions into (3) and (4) and evaluating the sums gives

$$c_a^0 = K_{da}(\eta - \zeta) + \frac{K_{da} K_{df}}{K_d} \zeta + 2K_2 K_{da}^2 \eta^2 + 3K_3 K_{da}^3 \eta^3 \\ + \frac{K_4 K_{da}^4 \eta^3 (4 - 3\eta)}{(1 - \eta)^2} \left(\eta - \left(1 - \frac{K_{df}}{K_{db}} \right) \zeta \right), \quad (10)$$

$$c_w^0 = K_{df} \frac{\zeta}{\eta - \zeta} + \frac{K_{da} K_{df}}{K_d} \zeta + 2K_2 K_{da}^2 \eta \zeta + 3K_3 K_{da}^3 \eta^2 \zeta \\ + \frac{K_4 K_{da}^4 \eta^2 \zeta}{(1 - \eta)^2} \left((\eta - \zeta)(3 - 2\eta) + \frac{K_{df}}{K_{db}} [\eta(1 - \eta) + \zeta(3 - 2\eta)] \right), \quad (11)$$

where we have defined

$$\eta \equiv \frac{c_a}{K_{da}} \left(1 + \frac{c_w}{K_{df}} \right) \quad (12)$$

$$\text{and } \zeta \equiv \frac{c_a c_w}{K_{da} K_{df}}. \quad (13)$$

We numerically solve for η and ζ , which gives the steady state concentrations of all species via (5)-(9). Applying the constraints that $0 < \zeta < \eta < 1$ ensures that all sums converge and that all concentrations are positive.

The pyrene fluorescence intensity is a function of the fraction of actin monomers that are in a filament, f_{fil} . Once η and ζ are determined, this is calculated as

$$f_{\text{fil}} = \frac{1}{c_a^0} (c_a^0 - c_a - c_{aw}) = 1 - \frac{K_{da}}{c_a^0} \left(\eta - \left(1 - \frac{K_{df}}{K_d} \right) \zeta \right). \quad (14)$$

We assume that the pyrene signal varies linearly with f_{fil} :

$$f_{\text{fil}} = \frac{p - p_{\text{bg}}}{p_0 - p_{\text{bg}}}, \quad (15)$$

where p is the measured pyrene signal, p_{bg} is the background pyrene signal, and p_0 is the pyrene signal we would observe if all actin monomers were incorporated into filaments. We cannot measure p_0 , but we assume it is linear in the total amount of labeled actin, or

$$p_0 - p_{\text{bg}} = \tilde{p} c_a^0, \quad (16)$$

where \tilde{p} is the constant of proportionality. Thus,

$$p = p_{\text{bg}} + \tilde{p} c_a^0 f_{\text{fil}}. \quad (17)$$

In the case where there is no binding of WH2 domains in filaments, $K_{df}, K_{db} \rightarrow \infty$, $\zeta = 0$ and (10)

and (11) simplify to a single equation.

$$c_a^0 = K_{da}\eta + \frac{K_{da}\eta}{K_d + K_{da}\eta} c_w^0 + 2K_2 K_{da}^2 \eta^2 + 3K_3 K_{da}^3 \eta^3 + \frac{K_4 K_{da}^4 \eta^4 (4 - 3\eta)}{(1 - \eta)^2}, \quad (18)$$

where we now have $\eta = c_a/K_{da}$. This equation gives a sixth order polynomial in η , which may be solved using a regular perturbation analysis. Inserting the perturbation solution into (14) and (17) yields

$$p = \begin{cases} p_{bg} + \tilde{p} \left[c_a - K_{da} \left(1 + \frac{c_w^0}{K_d + K_{da}} \right) \right] & \text{if } c_w^0 < \left(1 + \frac{K_d}{K_{da}} \right) (c_a^0 - K_{da}) \\ p_{bg} & \text{otherwise,} \end{cases} \quad (19)$$

where we have neglected terms of order $(K_{da}/c_a^0)^{\frac{3}{2}}$ and higher in the top expression and terms of order $(K_{da}/c_w^0)^2$ and higher in the bottom. This gives a well-defined ‘‘corner concentration’’ in the SSPT curve, given by

$$c_w^{\text{corner}} = \left(1 + \frac{K_d}{K_{da}} \right) (c_a^0 - K_{da}). \quad (20)$$

Note that the corner concentration is entirely determined by previously measured parameters.

Supplemental Methods

All constructs were transformed into *E. coli* BL21(DE3) cells (New England Biolabs, Ipswich, MA), and cultured in 1L TB media until an OD₆₀₀ of 0.8 was reached. Expression was induced by adding isopropyl-β-D-thiogalactopyranoside (IPTG) at 150-250 μM. Cells transformed with single WH2-containing constructs shook for 18–20 h at 18°C post induction. Cells expressing WH2-L3-WH2 constructs shook for 3 h at 37°C. Cells were harvested by centrifugation and pellets were resuspended in 15 mL of PBS (10 mM Na₂HPO₄, 1.8 mM KH₂PO₄, 140 mM NaCl, 2.7 mM KCl, pH 7.0) and centrifuged again before they were flash frozen and stored at -80°C.

Thawed cell pellets were resuspended in lysis buffer (PBS supplemented with 1 mM dithiothreitol (DTT), 1.7 mM phenylmethanesulfonyl fluoride (PMSF) and 1 μg/mL DNaseI. All subsequent steps were carried out at 4°C or on ice. Cells were lysed by two passages through a microfluidizer (Microfluidics, Newton, MA). The lysate was centrifuged at 20,000 × g for 20 min, and the supernatant was rocked with 1.5 mL glutathione–Sepharose 4b resin (GE Healthcare) for 1 h. Eluate was dialyzed in PBS supplemented with 1 mM DTT for 2 h at 4°C before the constructs were cleaved from GST by incubating them with 1-5% (w/v) PreScission protease overnight at 4°C. Both protease and cleaved GST were removed by rocking with fresh glutathione–Sepharose 4b resin for 1 h. The unbound fraction from the glutathione–Sepharose 4b resin was then dialyzed against 10 mM Tris pH8, 100 mM KCl, and 1mM DTT, and further purified through anion exchange (MonoQ, GE Healthcare) by collecting the flow through. Fractions were pooled together and dialyzed against 10mM Tris pH 8.0, and 1mM DTT overnight at 4°C. Protein aliquots were flash-frozen in liquid nitrogen and stored at -80°C.

Due to a tendency to degrade, WH2C and WH2C[QE] were purified and frozen in one day. Modification to this purification method were made for constructs that contained a His-tag (see Table S2.1) in that these constructs were isolated from the cleaved GST and protease via TALON purification (Clontech, Mountain View, CA). All multiple WH2 domain containing constructs were dialyzed into 20 mM HEPES pH 8.0, 100 mM KCl, and 1mM DTT, and further purified through cation exchange (MonoS, GE Life Sciences). Individual WH2 constructs were further purified through anion exchange as explained above. We were unable to purify WH2A by these methods, therefore it was synthesized by Biomatik USA, LLC.

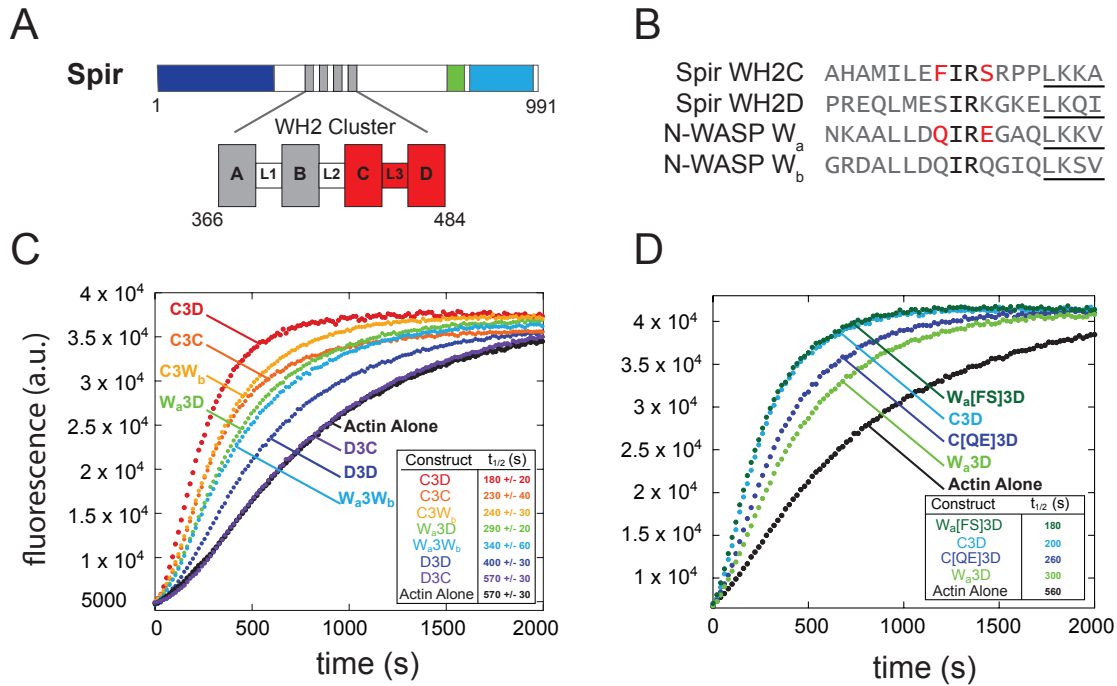


Figure 2.1: Domain order and key residues affect nucleation (A) Schematic of *Drosophila* Spir domain structure: KIND, kinase noncatalytic C-lobe domain (dark blue), WH2, Wasp homology-2 cluster (grey and expanded), Spir box (green), mFYVE, modified Fab1/YOTB/Vac1/EEA1 zinc-binding domain (light blue) and minimal nucleation construct (red in expanded WH2 cluster). (B) Alignment of the core region of the last two WH2 domains of *Drosophila* Spir and the two WH2 domains of *R. rattus* N-Wasp. Mutated residues are red and conserved isoleucines and arginines are black. A line is drawn below the LKKT/V motif. (C) Representative traces of actin polymerization assays monitored by pyrene fluorescence. Minimal nucleation construct variants (0.25 μ M) were added to 4 μ M actin. (D) Gain of function point mutations convert W_a3D into a construct as potent as C3D (W_a[FS]3D). The converse mutations in C3D (C[QE]3D) result in loss of activity.

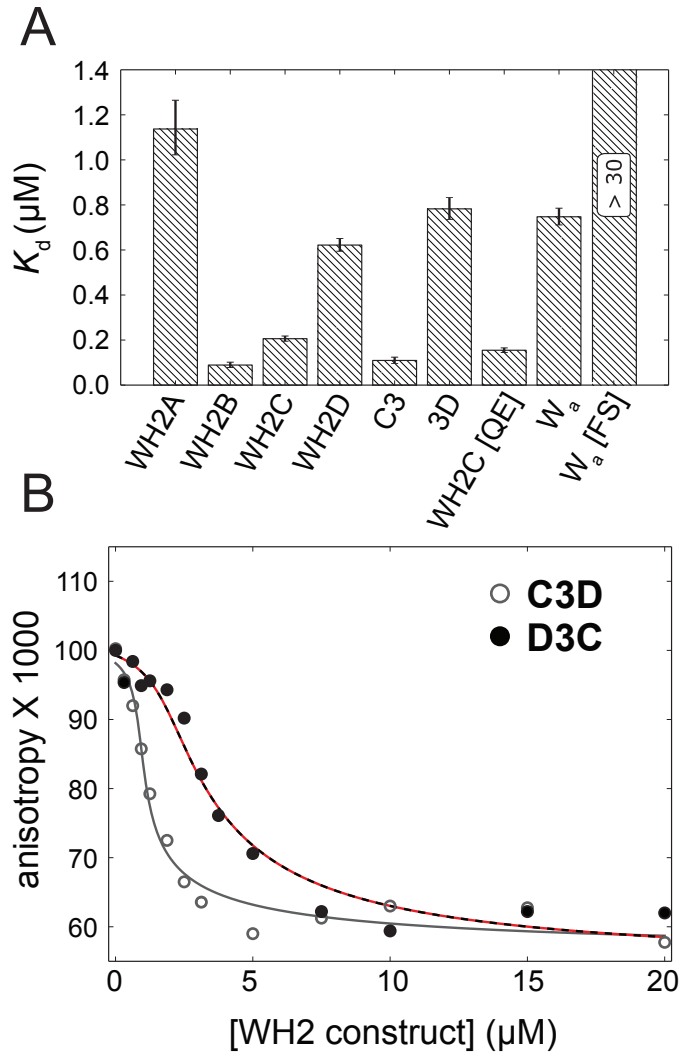


Figure 2.2: WH2 domains synergistically bind monomeric actin. (A) The reported K_d values of WH2 constructs bound to latB-actin are the mean of three independent trials of competition fluorescence anisotropy with WH2D-AlexaFluor488 (Figure S2.1). W_a [FS] binds too weakly to determine the affinity. Error bars represent one standard deviation. (B) Representative competition fluorescence anisotropy with WH2D-AlexaFluor488 and latB-actin as a function of added C3D (filled circles) or D3C (open circles). Data are fit with a two-site equilibrium binding model. Regressions are in the same color as the data set and the dashed red line represents modeling assuming the K_d for a second monomer is infinite.

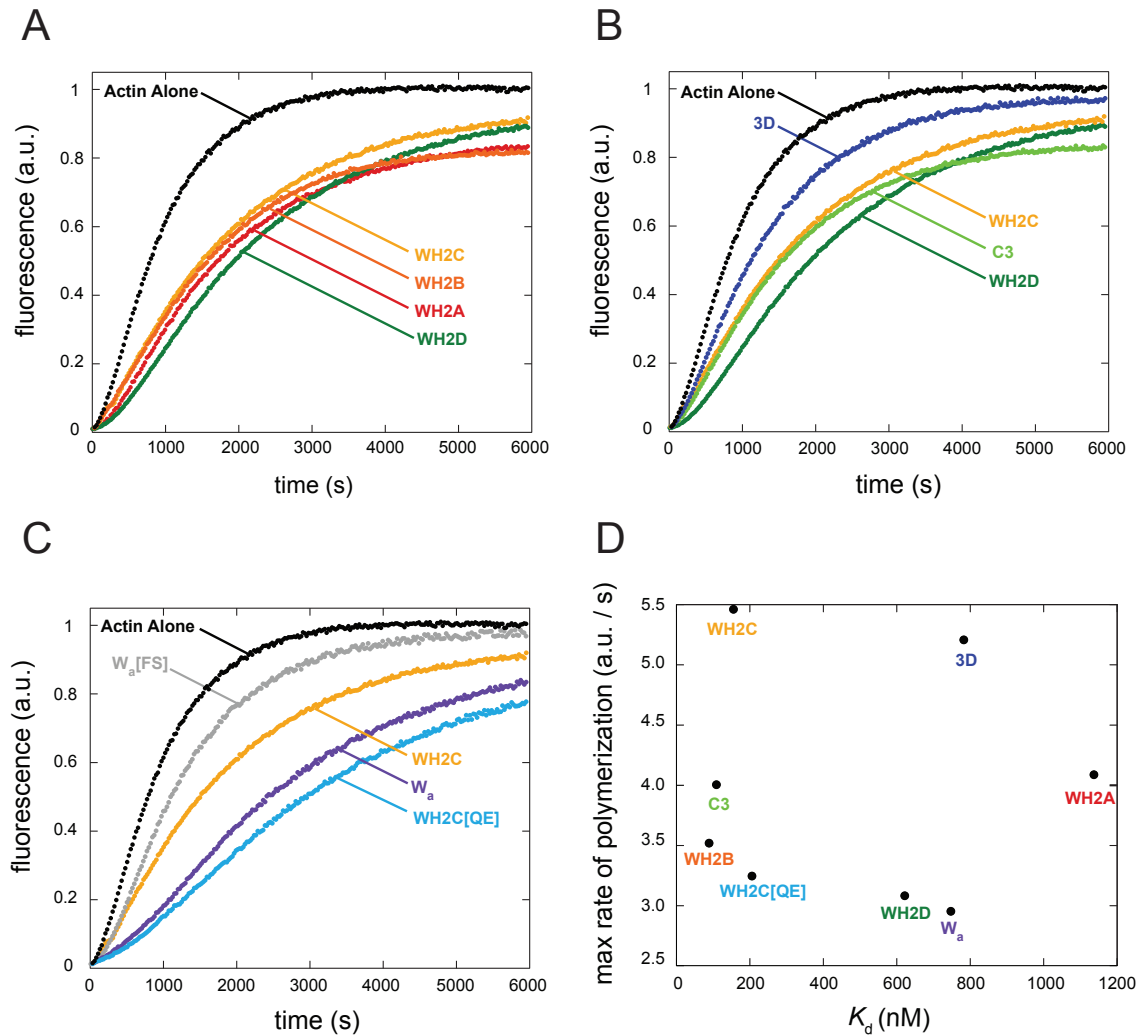


Figure 2.3: Inhibition of spontaneous actin polymerization by WH2 domains does not correlate with actin binding affinity. (A) Representative traces of actin polymerization in the presence of the four wild-type Spir-WH2 domains group together despite very different affinities for actin. (B) Adding Linker 3 has little effect on WH2C but markedly decreases inhibition by WH2D. (C) Mutations in W_a decrease inhibition, making it behave more like WH2C and mutations in WH2C increase inhibition, making it behave more like W_a . (A-C) 3 μ M WH2 added to 4 μ M actin is shown in all cases. (B) Scatter plot of maximum rates from (A-C) versus K_d . No correlation is seen.

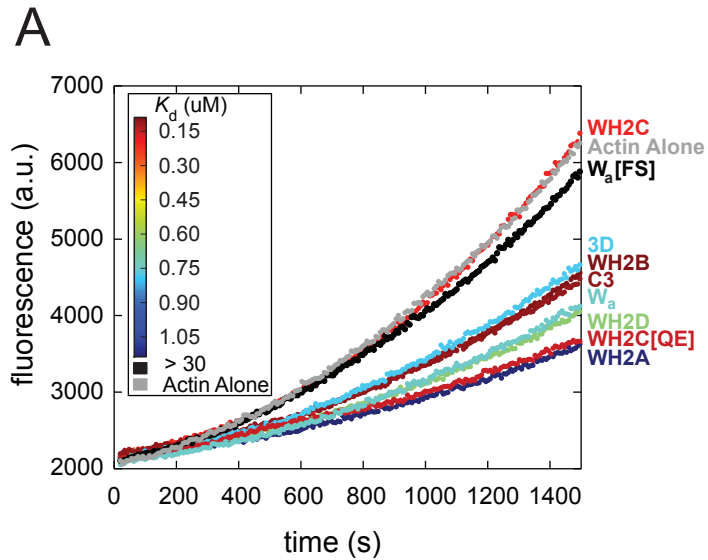


Figure 2.4: Effects of individual WH2 domains on actin nucleation. (A) Representative pyrene-actin polymerization assays of different WH2 domain constructs (1.5 μ M) added to actin (2 μ M) during nucleation. Each trace is colored according to the actin binding affinity of the added WH2 domain according to the inset heat map (red is high affinity). If the effect on nucleation correlated to affinity, the traces would have a rainbow-like trend, but it does not.

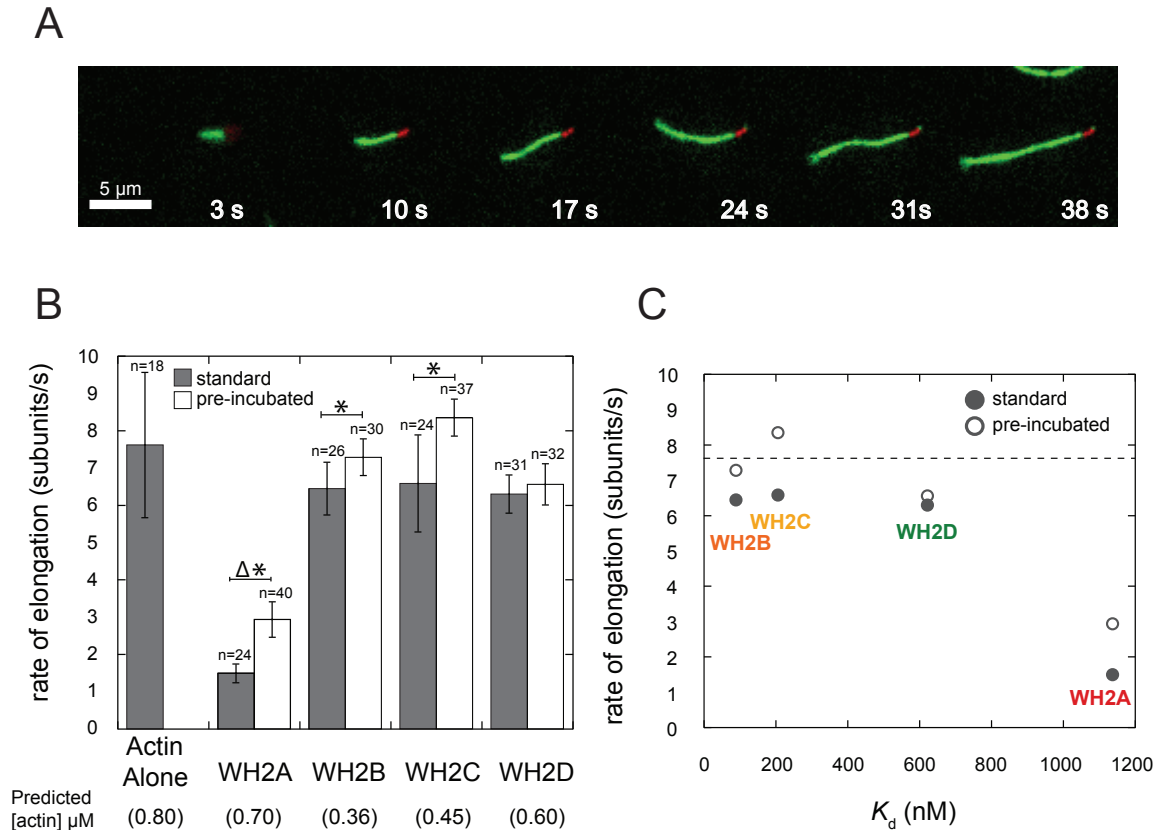


Figure 2.5: Elongation rates of actin determined by TIRF microscopy. (A) Example of seeded actin (red) and elongation (green) in the presence of WH2C observed by TIRF. (B) Actin elongation rates in the presence of 1 μ M of indicated individual WH2 domains with pre-incubation (grey) and without (white). The values in parentheses indicate the predicted concentration of free actin, given the K_d 's determined in this study. Symbols Δ (comparing with actin alone) and * (comparing standard and pre-incubated conditions) indicate statistical significance ($p < 0.01$). (n is the number of filaments analyzed for each case; error bars are one standard deviation) (C) Elongation rates of each WH2 domain determined in B and plotted as a function of affinity for actin.

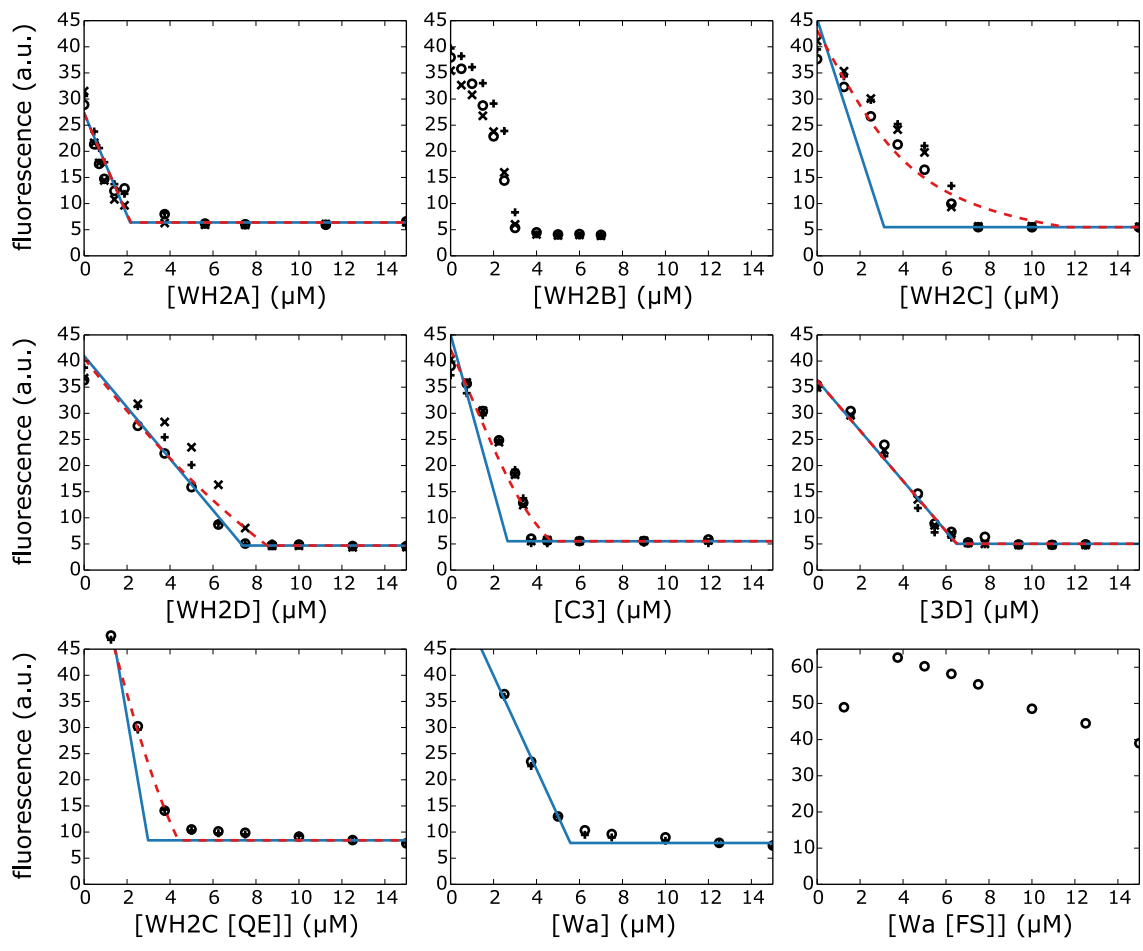


Figure 2.6: Effect of individual WH2 domains on actin at steady state. Raw data and analysis of steady state polymerization titration (SSPT) assays for all nine constructs are shown. Each concentration was tested three times and is represented by different symbols. Predicted values based on the model described in the appendix, with K_d fixed by our anisotropy measurements, are shown in blue. Extending this model to include filament side binding (K_{df}) is shown in red. Due to extremely weak binding, we could not analyze the W_a [FS] curves. WH2B was not analyzed because it did not reach steady state, as evidenced by the concavity of the titration curves. No red trace is shown for W_a because the regression did not converge.

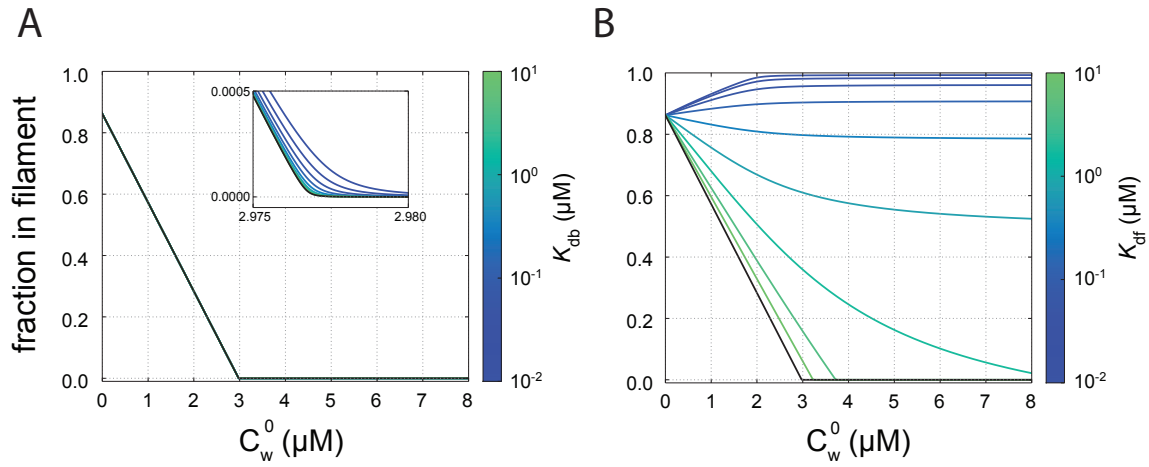


Figure 2.7: Effects of K_{db} and K_{df} on steady state actin polymerization. For these illustrative curves, K_{da} is that determined for 10% pyrene-labeled actin and $K_d = 0.2 \mu\text{M}$. The black curves have K_{db} or $K_{df} \rightarrow \infty$. (A) SSPT curves for various values of K_{db} with $K_{df} \rightarrow \infty$. (B) SSPT curves for various values of K_{df} .

WH2 Constructs	ΔrG^d (kJ/mol)	K_d (μ M)	Elongation rate		max rate at 3 μ M (a.u.)	ΔrG^{df} (kJ/mol)	K_d^{df} (μ M)	Inhibition of nucleation	Inhibition of nucleation w/ pre-incubation
			rate (sub/s)	w/ pre-incubation (sub/s)					
WH2A	-0.3 \pm 0.3	1.14	1.5 \pm 0.2	2.9 \pm 0.4	4.1 \pm 0.5	-8 \pm 3	28	+++	++
WH2B	5.9 \pm 0.3	0.09	6.5 \pm 0.7	7.3 \pm 0.5	3.5 \pm 0.4	N/D	N/D	++	-
WH2C	3.9 \pm 0.1	0.21 (0.01)	6.6 \pm 1.3	8.4 \pm 0.5	3.1 \pm 0.1	-1.6 \pm 0.3	2.0	-	-
WH2D	1.2 \pm 0.1	0.62 (0.03)	6.3 \pm 0.5	6.6 \pm 0.5	3.2 \pm 0.4	-6.2 \pm 0.6	13	+++	+++
C3	5.4 \pm 0.3	0.11	N/D	N/D	4.0 \pm 0.3	-0.9 \pm 0.5	1.4	++	++
3D	0.6 \pm 0.2	0.78	N/D	N/D	5.2 \pm 0.7	-15 \pm 5	500	+	+
WH2C[QE]	4.6 \pm 0.2	0.15	N/D	N/D	2.1 \pm 0.2	-1.6 \pm 0.4	1.9	+++	+++
W_a	0.7 \pm 0.1	0.75	N/D	N/D	3.0 \pm 0.3	##	##	++	++
W_a [FS]	*	*	N/D	N/D	5.5 \pm 0.4	N/D	N/D	-	-

The values in parentheses are the predicted K_d 's for a second actin monomer binding to C3D as described for Figure 2B.

* W_a [FS] affinity is too weak to determine with confidence. It is > 30 μ M.

##Regression for W_a with K_d^{df} free did not converge.

N/D = not determined.

Table 2.1: Summary of results.

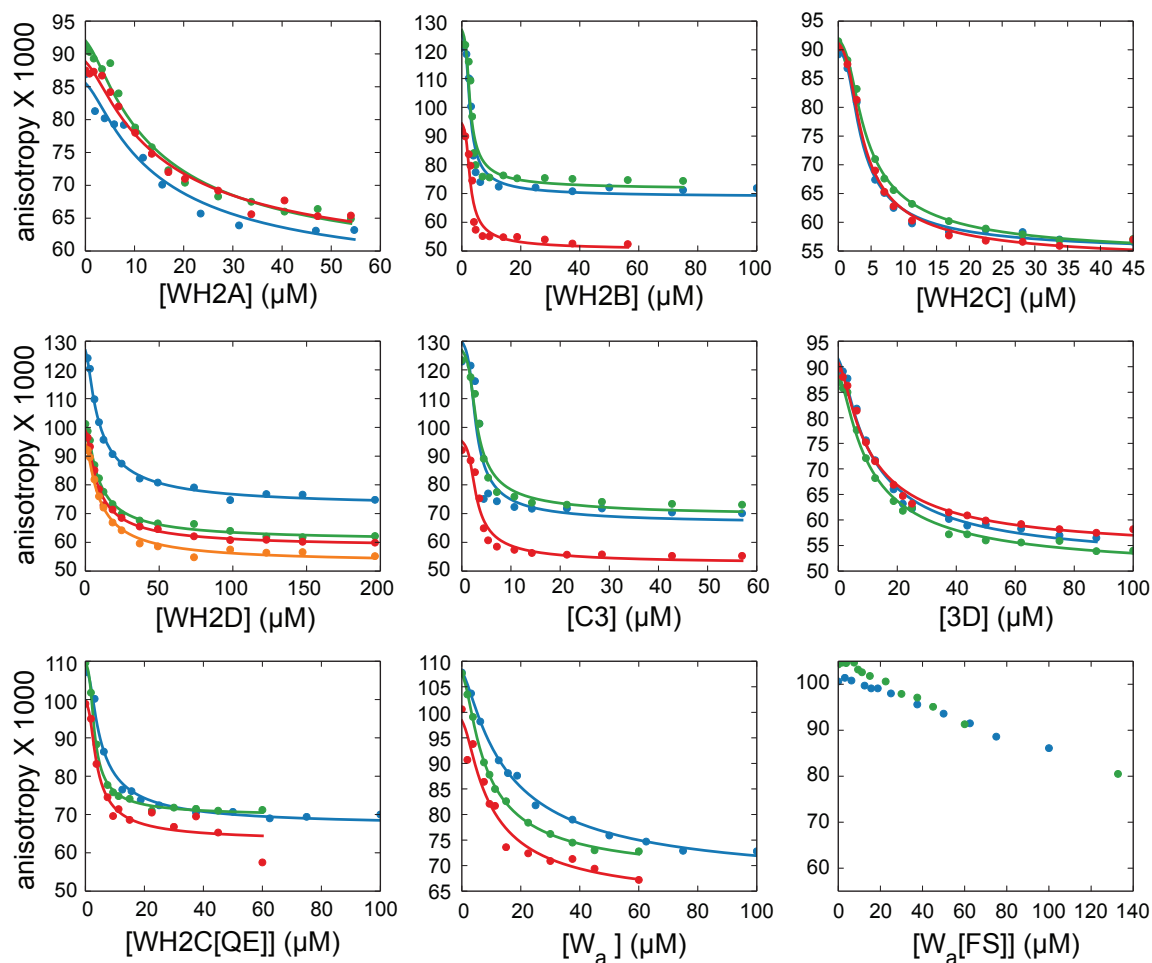


Figure S2.1: Fluorescence anisotropy experiments of each WH2 domain construct. Each regression was performed independently. Like colors are regressions of respective data sets. Average affinities from these three trials are reported in Figure 2.2 and Table 2.1.

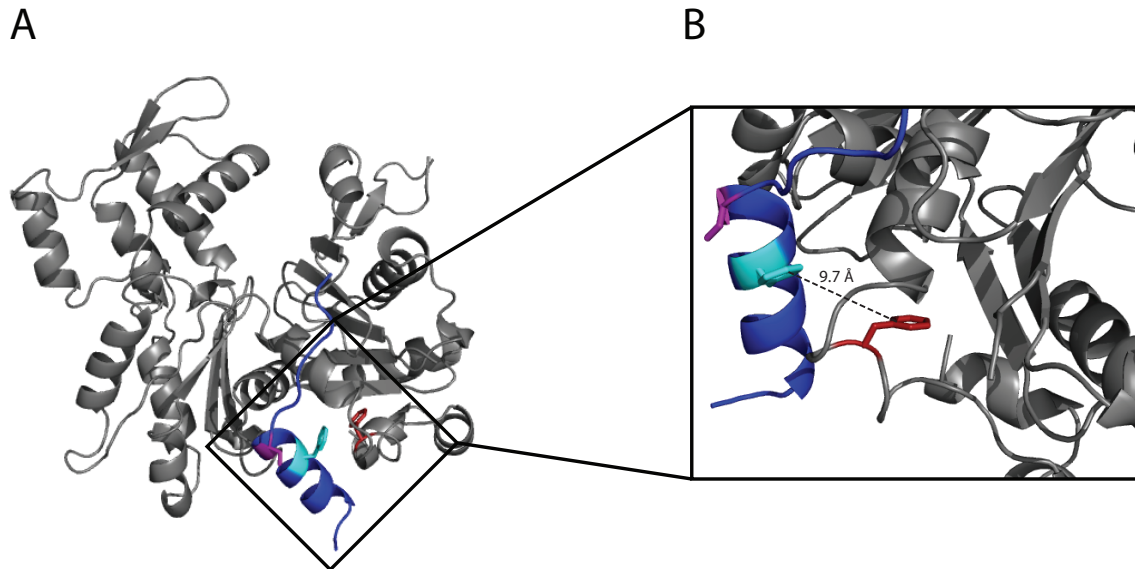


Figure S2.2: Homology model of Spir WH2C and actin co-crystal: (A) Spir WH2C domain (blue) replaces WH2D in a co-crystal with *A. castellani* actin (grey) pdb: 4EFH. Actin Phe-352 (red) is part of an unstructured loop and with minimal rearrangements may stack with WH2C Phe-438 (cyan). Because it is small and uncharged, WH2C Ser-441 (purple) allows for this rearrangement, contributing to the Phe stacking and deeper placement of WH2C into the actin hydrophobic pocket. (B) Zoom in box region from (A). The dashed line represents the distance between WH2C Phe-438 and actin Phe-352.

Construct name	Amino Acid Sequence
WH2A	WARFWVQVIDELRRGVRLKKSNER
WH2B	GPLGSELTPYEILMGDIRAKKYQLRKVMVNGAAAS
WH2C	GPLGSKKDAHAMILEFIRSRPPLKKASDRQAAAS
WH2D	GPLGSEPSPREQLMESIRKGKELKQITPPEAAAS
WH2D-KCK	GPLGSEPSPREQLMESIRKGKELKQITPPEKCK
WH2C-L3	GPLGSKKDAHAMILEFIRSRPPLKKASDRQLGPPRMCEPSHHHHHH
L3-WH2D	GPLGSASDRQLGPPRMCEPSPREQLMESIRKGKELKQITPPE
WH2C[QE]	GPLGSKKDAHAMILEQIRERPPLKKASDRQAAAS
wa	GPLGSGNKAALLDQIREGAQLKKASDRQLGAAAS
wa[FS]	GPLGSGNKAALLDFIRSGAQLKKASDRQLGAAAS
C3D	GPLGSKKDAHAMILEFIRSRPPLKKASDRQLGPPRMCEPSPREQLMESIRKGKELKQITPPEAAAS
C3C	GPLGSKKDAHAMILEFIRSRPPLKKASDRQLGPPRMCEPSAHAMILEFIRSRPPLKKASDRQHHHHHH
D3D	GPLGSEPSPREQLMESIRKGKELKQASDRQLGPPRMCEPSPREQLMESIRKGKELKQITPPEHHHHHH
wa3D	GPLGSGNKAALLDQIREGAQLKKASDRQLGPPRMCEPSPREQLMESIRKGKELKQITPPEAAAS
wa3wb	GPLGSGNKAALLDQIREGAQLKKASDRQLGPPRMCEPSGRDALLDQIRQGIQLKSVSDGQAAAS
D3C	GPLGSEPSPREQLMESIRKGKELKQASDRQLGPPRMCEPSAHAMILEFIRSRPPLKKASDRQHHHHHH
C3wb	GPLGSKKDAHAMILEFIRSRPPLKKASDRQLGPPRMCEPSGRDALLDQIRQGIQLKSVSDGQAAAS
C[QE]3D	GPLGSKKDAHAMILEQIRERPPLKKASDRQLGPPRMCEPSPREQLMESIRKGKELKQITPPEAAAS
wa[FS]3D	GPLGSGNKAALLDFIRSGAQLKKASDRQLGPPRMCEPSPREQLMESIRKGKELKQITPPEAAAS

Table S2.1: WH2 Constructs. This table includes the names (left) and amino acid sequences (right) of all the constructs used. Residues in the grey boxes remain after GST cleavage (GPLGS), are due to cloning strategy (AAAS), added for labeling (KCK), or a His-tag needed for purification.

References

- [1] Chereau, D., F. Kerff, P. Graceffa, Z. Grabarek, K. Langsetmo, and R. Dominguez Actin-bound structures of Wiskott-Aldrich syndrome protein (Wasp)-homology domain 2 and the implications for filament assembly. *Proc Natl Acad Sci U S A* 2005;102:16644-16649.
- [2] Chen, C.K., M.R. Sawaya, M.L. Phillips, E. Reisler, and M.E. Quinlan Multiple forms of Spire-actin complexes and their functional consequences. *J Biol Chem* 2012;287:10684-10692.
- [3] Ducka, A.M., et al. Structures of actin-bound Wiskott-Aldrich syndrome protein homology 2 (WH2) domains of Spire and the implication for filament nucleation. *Proc Natl Acad Sci U S A* 2010;107:11757-11762.
- [4] Rebowski, G., S. Namgoong, M. Boczkowska, P.C. Leavis, J. Navaza, and R. Dominguez Structure of a longitudinal actin dimer assembled by tandem w domains: implications for actin filament nucleation. *J Mol Biol* 2010;403:11-23.
- [5] Aguda, A.H., B. Xue, E. Irobi, T. Preat, and R.C. Robinson The structural basis of actin interaction with multiple WH2/beta-thymosin motif-containing proteins. *Structure* 2006;14:469-476.
- [6] Hertzog, M., et al. The beta-thymosin/WH2 domain; structural basis for the switch from inhibition to promotion of actin assembly. *Cell* 2004;117:611-623.
- [7] Lee, S.H., F. Kerff, D. Chereau, F. Ferron, A. Klug, and R. Dominguez Structural basis for the actin-binding function of missing-in-metastasis. *Structure* 2007;15:145-155.
- [8] Didry, D., et al. How a single residue in individual beta-thymosin/WH2 domains controls their functions in actin assembly. *EMBO J* 2012;31:1000-1013.
- [9] Ahuja, R., et al. Cordon-bleu is an actin nucleation factor and controls neuronal morphology. *Cell* 2007;131:337-350.
- [10] Quinlan, M.E., J.E. Heuser, E. Kerkhoff, and R.D. Mullins *Drosophila* Spire is an actin nucleation factor. *Nature* 2005;433:382-388.
- [11] Zuchero, J.B., A.S. Coutts, M.E. Quinlan, N.B. Thangue, and R.D. Mullins p53-cofactor JMY is a multifunctional actin nucleation factor. *Nat Cell Biol* 2009;11:451-459.
- [12] Qualmann, B. and M.M. Kessels New players in actin polymerization--WH2-domain-containing actin nucleators. *Trends Cell Biol* 2009;19:276-285.
- [13] Manseau, L.J. and T. Schupbach cappuccino and spire: two unique maternal-effect loci required for both the anteroposterior and dorsoventral patterns of the *Drosophila* embryo. *Genes Dev* 1989;3:1437-1452.
- [14] Ravanelli, A.M. and J. Klingensmith The actin nucleator Cordon-bleu is required for development of motile cilia in zebrafish. *Dev Biol* 2011;350:101-111.
- [15] Wang, Q.C., et al. Role of nucleation-promoting factors in mouse early embryo development. *Microsc Microanal* 2013;19:559-564.
- [16] Carroll, E.A., et al. Cordon-bleu is a conserved gene involved in neural tube formation. *Dev Biol* 2003;262:16-31.
- [17] Ferreira, T., Y. Ou, S. Li, E. Giniger, and D.J. van Meyel Dendrite architecture organized by transcriptional control of the F-actin nucleator Spire. *Development* 2014;141:650-660.
- [18] Liverman, A.D., et al. Arp2/3-independent assembly of actin by *Vibrio* type III effector VopL. *Proc Natl Acad Sci U S A* 2007;104:17117-17122.
- [19] Tam, V.C., D. Serruto, M. Dziejman, W. Brieher, and J.J. Mekalanos A type III secretion system in *Vibrio cholerae* translocates a formin/spire hybrid-like actin nucleator to promote intestinal colonization. *Cell Host Microbe* 2007;1:95-107.

- [20] Pfender, S., V. Kuznetsov, S. Pleiser, E. Kerkhoff, and M. Schuh Spire-type actin nucleators cooperate with Formin-2 to drive asymmetric oocyte division. *Curr Biol* 2011;21:955-960.
- [21] Bosch, M., K.H. Le, B. Bugyi, J.J. Correia, L. Renault, and M.F. Carlier Analysis of the function of Spire in actin assembly and its synergy with formin and profilin. *Mol Cell* 2007;28:555-568.
- [22] Zahm, J.A., et al. The bacterial effector VopL organizes actin into filament-like structures. *Cell* 2013;155:423-434.
- [23] Quinlan, M.E., S. Hilgert, A. Bedrossian, R.D. Mullins, and E. Kerkhoff Regulatory interactions between two actin nucleators, Spire and Cappuccino. *J Cell Biol* 2007;179:117-128.
- [24] Vizcarra, C.L., et al. Structure and function of the interacting domains of Spire and Fmn-family formins. *Proc Natl Acad Sci U S A* 2011;108:11884-11889.
- [25] Horton, R.M. PCR-mediated recombination and mutagenesis. SOEing together tailor-made genes. *Mol Biotechnol* 1995;3:93-99.
- [26] MacLean-Fletcher, S. and T.D. Pollard Identification of a factor in conventional muscle actin preparations which inhibits actin filament self-association. *Biochem Biophys Res Commun* 1980;96:18-27.
- [27] Cooper, J.A., S.B. Walker, and T.D. Pollard Pyrene actin: documentation of the validity of a sensitive assay for actin polymerization. *J Muscle Res Cell Motil* 1983;4:253-262.
- [28] Bor, B., C.L. Vizcarra, M.L. Phillips, and M.E. Quinlan Autoinhibition of the formin Cappuccino in the absence of canonical autoinhibitory domains. *Mol Biol Cell* 2012;23:3801-3813.
- [29] Zalevsky, J., I. Grigorova, and R.D. Mullins Activation of the Arp2/3 complex by the *Listeria acta* protein. Acta binds two actin monomers and three subunits of the Arp2/3 complex. *J Biol Chem* 2001;276:3468-3475.
- [30] Bois, J.S., *Analysis of Interacting Nucleic Acids in Dilute Solutions*, in *Ph.D. thesis*. 2007, California Institute of Technology.
- [31] Dirks, R.M., J.S. Bois, J.M. Schaeffer, and W. Winfree Thermodynamic analysis of interacting nucleic acid strands. *SIAM Review* 2007;49:65-88.
- [32] Smith, M.B., H. Li, T. Shen, X. Huang, E. Yusuf, and D. Vavylonis Segmentation and tracking of cytoskeletal filaments using open active contours. *Cytoskeleton (Hoboken)* 2010;67:693-705.
- [33] Schindelin, J., et al. Fiji: an open-source platform for biological-image analysis. *Nat Methods* 2012;9:676-682.
- [34] Arnold, K., L. Bordoli, J. Kopp, and T. Schwede The SWISS-MODEL workspace: a web-based environment for protein structure homology modelling. *Bioinformatics* 2006;22:195-201.
- [35] Pettersen, E.F., et al. UCSF Chimera--a visualization system for exploratory research and analysis. *J Comput Chem* 2004;25:1605-1612.
- [36] Sept, D. & McCammon, J. Thermodynamics and kinetics of actin filament nucleation. *Biophysical J* 2001;81:667-674.

Chapter 3: Preliminary data further characterizing Spir WH2C

Results

In the previous chapter we showed that the sequence of WH2C and its position relative to Linker 3 are critical for the nucleation activity of Spir. We also found that WH2C binds to actin filaments with an affinity of 2 μ M, which is an interaction previously unknown for any WH2 domain. In this chapter, I discuss additional work we performed investigating how WH2C contributes to Spir's nucleation activity. With the help of Grant Shoffner, we set up co-crystallization screens using numerous conditions to identify how WH2C and Linker 3 bind with actin, and whether the interaction differs from previously crystallized WH2 domains bound to actin. Second, with the help of Jesmine Cheung, we investigated the impact of sequence changes in the bridge of WH2 domains, the region in between the alpha helix and the LKK motif, has on nucleation activity.

Crystallography

The data presented so far supports a unique role for WH2C as being specialized for nucleation, which differs from canonical WH2-actin interactions. A structure of this interaction could provide a deeper understanding of how WH2C contributes to Spir's nucleation activity. Thus far WH2D bound to actin is the only Spir WH2 domain structure solved [1, 2]. As expected, WH2D followed a binding mode similar to that seen in previous WH2 domain/actin co-crystal structures, solved from a variety of proteins (Figure 2.1) [3-7]. Chen *et al.*, was able to solve two structures of a Spir WH2 C3D/actin complex but in both cases WH2C was not visible [1]. Our recent discovery that WH2C interacts uniquely with actin provides some potential insight into why they only observed WH2D bound to actin. This result, in combination with our findings from the previous chapter has further motivated our interest in solving a co-crystal of both WH2C and C3 bound to actin.

We used two approaches to prevent actin from polymerizing during our experiments. First, we used actin bound by latrunculin A (latA) at a molar ratio of 2:1. The latrunculin family of toxins bind to actin monomers near the nucleotide binding cleft in a 1:1 stoichiometry and prevent them from polymerizing. Next we used actin bound to Deoxyribonuclease I (DNase I) at a molar ratio of 1.5:1. DNase I also binds to actin in a 1:1 stoichiometry, but targets subdomain 2 to block polymerization. These techniques have been widely used in the field to successfully solve actin co-crystals. We set up a number of screens with inhibitor-bound actin and Spir constructs WH2C, C3, or C3D at a ratio of 4:1 WH2 to actin (Table 2.1). Vizcarra *et al.* had previously shown that Spir nucleation activity is enhanced when dimerized with GST, so we also used a GST tagged construct of C3D in order to mimic a dimer in hopes that this stabilization would increase the chance of crystallization [8].

Multiple conditions led to crystal formation, but the most successful one included WH2C3/latA-actin in 0.1 M CHES, pH 9.5, with 0.91 M citrate (Table 2.2). This condition produced a crystal, which diffracted to a resolution of 3.7 Å (Figure 2.1). Through the use of molecular replacement and a previously solved structure of actin, we observed a mass in the hydrophobic cleft of actin that we could assign to WH2C (Figure 3.2). Unfortunately, due to the limits of resolution we could not assign density to the side chains and so further work is needed to obtain the desired resolution.

The Bridge

We call the region of a WH2 domain between the alpha helix and the LKK motif, the bridge (Figure 2.2 A, B). Didry *et al.*, used the proteins Thymosin-β4 (Tβ4) and Cibulout (Cib), which contain WH2-like domains, to show that changing a single residue in their bridge region can modify the interaction between actin and the WH2-like domain (Figure 2.2 A) [9]. The WH2-like domain in Tβ4 sequesters actin monomers thereby

preventing filament polymerization. This contrasts with the first WH2-like domain in Cib (CibD1), which binds to actin permissively, meaning it does not block actin barbed end assembly similar to profilin bound actin [9]. By replacing a glutamine in the bridge region of CibD1 with the corresponding lysine from T β 4, Didry and co-workers were able to turn the permissive CibD1 into an actin sequesterer with activity nearly identical to that of T β 4. When they crystalized this mutant and compared it to wild type CibD1, they found that both glutamine and lysine interact with Ala-144 and Glu-334 of actin, respectively, suggesting this contact can alter the functional interaction between a WH2 domain and actin [9]. Based on these experiments, we examined the bridge of WH2C to learn whether the bridge region is important for nucleation as well.

We first created two mutant C3D constructs by replacing the Pro-Pro in the bridge of WH2C with either Gly-Lys or Gly-Ser, named C3D[GK] and C3D[GS], respectively (Figure 2.2 A). In these mutants, the lysine and serine are in the same position as the lysine and glutamine in T β 4 and Cib1, respectively. We next tested these mutants in bulk pyrene-actin polymerization assays and saw very little difference in nucleation activity compared to wild type C3D (Figure 2.3). We believe that the length of the bridge in WH2C is too short for the replaced residues to potentially interact with actin's A144 and E334, since the bridge region in both CibD1 and T β 4 are each 6 residues long. We made 3 additional mutants to increase the length of the bridge to 6 residues, C3D[GKGS], C3D[GSGS], and a mutant, which replaced the whole bridge region of WH2C with the one from T β 4, C3D[T β 4]. We initially noticed that all three mutants showed a lowered plateau when compared to C3D in pyrene-actin polymerization assays suggesting that a longer bridge region allows for a new interaction with actin causing C3D to sequester actin (Figure 2.3). Interestingly, although we see greatest sequestration with C3D[GKGS] as we might predict, it had nucleation activity

greater than both C3D[GSGS] and wild type C3D. In addition, replacing the bridge in WH2C with the one from T β 4 reduced the nucleation activity of C3D (Figure 2.3). These data further validate that the specific sequence of the bridge can modulate a WH2 and actin interaction leading to functional changes and suggest that this interaction is important for nucleation as well.

We next used the chimera W_a3D from Chapter 1 to study the impact the bridge of WH2C has on nucleation activity. We replaced 3 out of 4 residues from the bridge in W_a with the corresponding residues from WH2C to make the mutant W_a3D[RPP]. We know from Chapter 1 that W_a3D is a weaker nucleator than C3D and with 2 point mutations inspired by WH2C becomes as active as C3D. We tested the nucleation activity of W_a3D[RPP] and compared it to that of C3D and W_a3D and found that these mutations also increased the nucleation activity almost to C3D levels (Figure 3.4). This data fits nicely with our previous data showing WH2C is unique and critical to Spir's nucleation activity.

Methods

Protein Purification

Drosophila Spir and *R. rattus* N-Wasp constructs were created by methods described in Chapter 1. The *A. castellani* actin and WH2 constructs were also purified as described in Chapter 1. We used DNaseI purchased from Bio-world (Catalog number: 215600081 (750050))

Pyrene-Actin Assembly Assays

Pyrene-actin assembly assays were carried out essentially as described in Chapter 1 using 4 μ M actin and 250 μ M WH2 constructs.

X-Ray Crystallography

Acanthamoeba actin was mixed with purified WH2C, C3, or GST-C3D Spir constructs at a 4:1 molar ratio. LatA-actin was made by mixing a 2-fold molar excess of latA with actin for 1 h at 25°C. Both DNaseI/actin/Spir WH2C and GST-C3D/latA-actin complexes were purified by gel filtration. The protein mixture was crystallized using the hanging drop method with a drop consisting of equal parts of protein and mother liquor. The commercial screen kits we used, Emerald Biosystems, Hampton Research, and Qiagen, were provided by the UCLA-DOE crystallization core. Crystal tray storage temperature and cryo-protectants used are described in Tables 3.1 and 3.2. X-ray diffraction data was collected in the UCLA-DOE crystallization core using a Rigaku FRE+ generator with 2 HTC detectors and varimax confocal optics. Crystals were cooled at 100 K by four X-tream Liquid Nitrogen cryogenic coolers. The crystals belonged to space group P1 with one actin monomer and one Spir C3 molecule in the asymmetric unit. 350 x 1.0° oscillation frames were collected with an exposure time of 300s and a distance between the detector and crystal of 180 mm. Diffraction to 3.7 Å was observed.

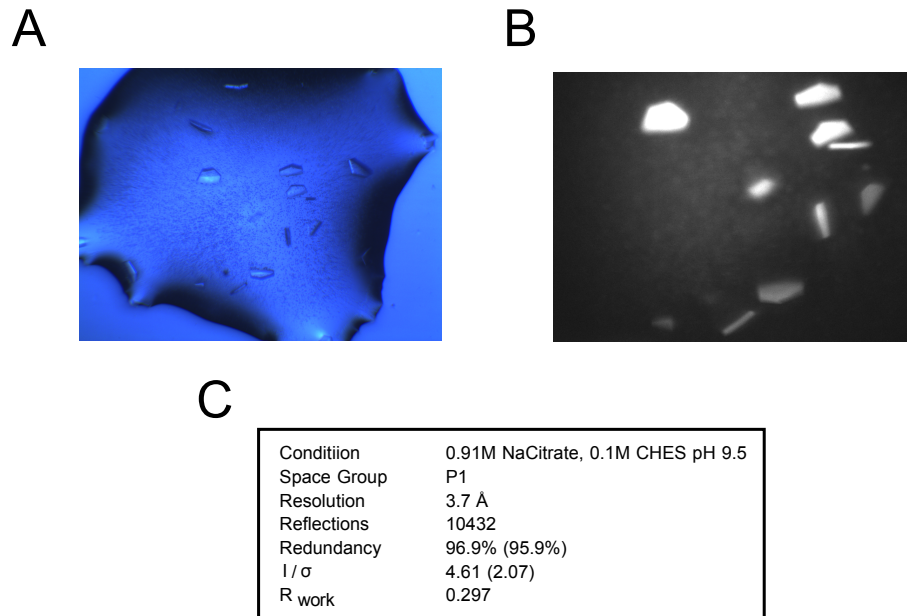


Figure 3.1: Spir C3 and actin co-crystals. Microscopy images under visible light (A) or ultraviolet fluorescence (B) of C3 / actin co-crystals. (C) Data collected from diffraction of C3 / actin co-crystals.

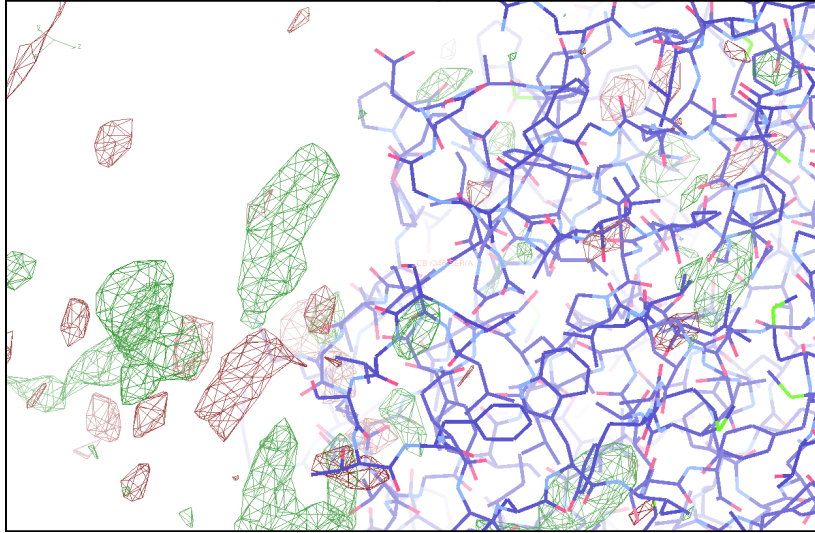


Figure 3.2: Electron Density Fo-Fc map. This density map was processed from the diffraction data collected in Figure 3.1 C. We used molecular replacement to model in the actin (blue sticks) and positive electron density from C3 atoms are shown in green and negative electron density is shown in red. C3 electron density is detected in the hydrophobic cleft of actin. The quality of diffraction needs to be improved.

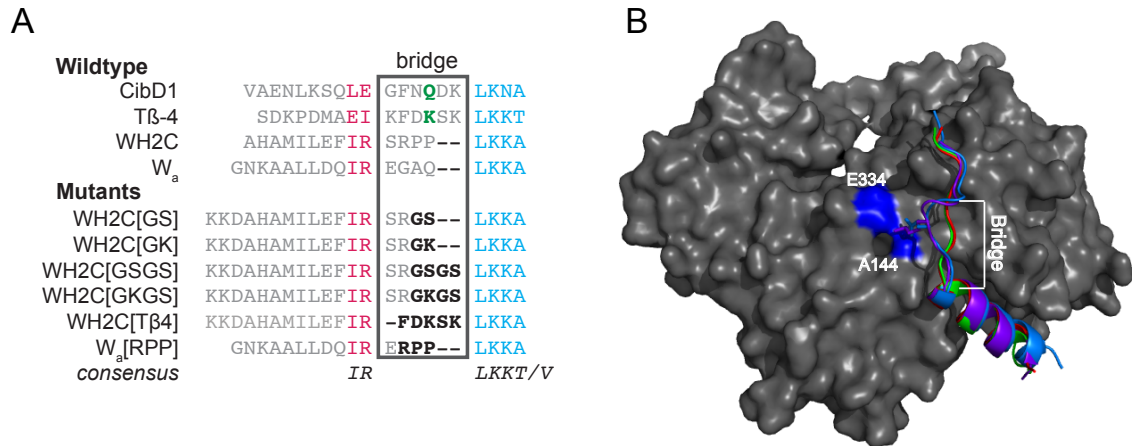


Figure 3.3: Mutations in the bridge region. (A) Sequences of the WH2-like domains from Cib, Tβ4 and WH2 domains from Spir WH2C, N-Wasp W_a and their mutated constructs. The bridge region is shown in the black box and conserved IR and LKK motifs shown in pink and blue, respectively. Green highlights the important residues from CibD1 and Tβ4 reported in Didry *et al.*, and black represents the mutated residues from this study [9]. (B) Crystal alignment of CibD1 (1SQK-Blue), a chimeric WH2-like domain comprised of the alpha helix from CibD1 and the bridge and LKK motif from Tβ4 (3U96-Purple), N-Wasp W_a (3M3N-Green), and Spir WH2D (4EFH-Red). Actin is in grey with blue highlighting residues E-334 and A-144. The side chains of residues in green (A) are shown as sticks in the model (B).

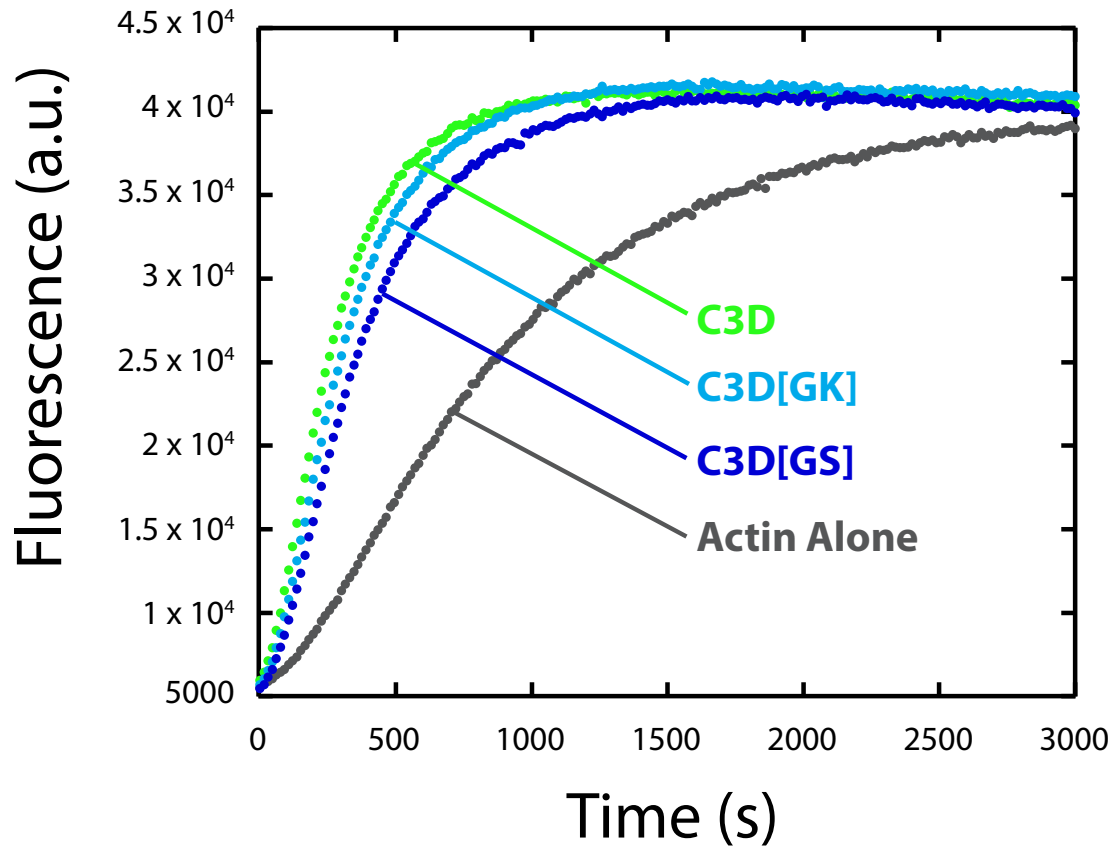


Figure 3.4: Two point mutations in the bridge of WH2C have a minimal affect on nucleation. Representative traces of actin polymerization in the presence of wild type C3D (green), or two mutants, C3D[GS] (dark blue) and C3D[GK] (light blue). Actin alone is shown in grey.

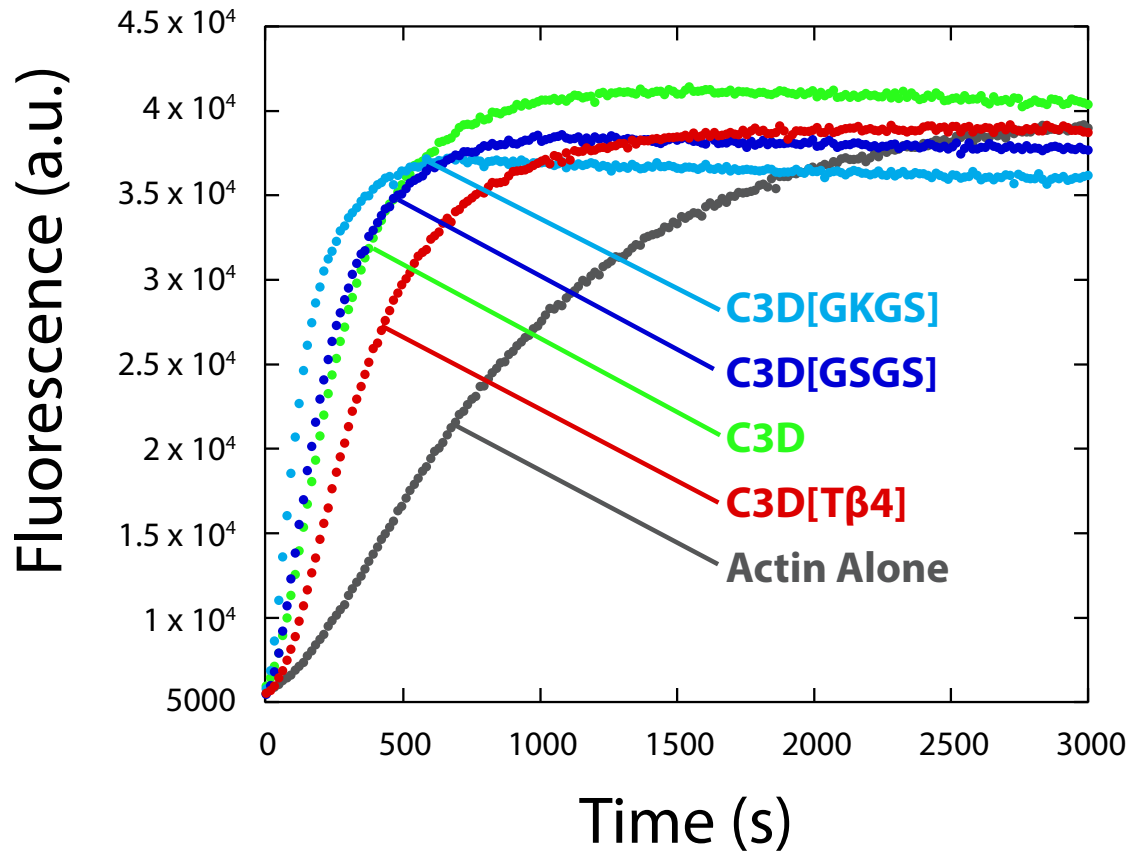


Figure 3.5: Mutating and elongating the bridge of WH2C changed its effect on actin polymerization. Representative traces of actin polymerization in the presence of wild type C3D (green), or three mutants, C3D[GSGS] (dark blue), C3D[GKGS] (light blue), and C3D[T β 4] (red). Actin alone is shown in grey.

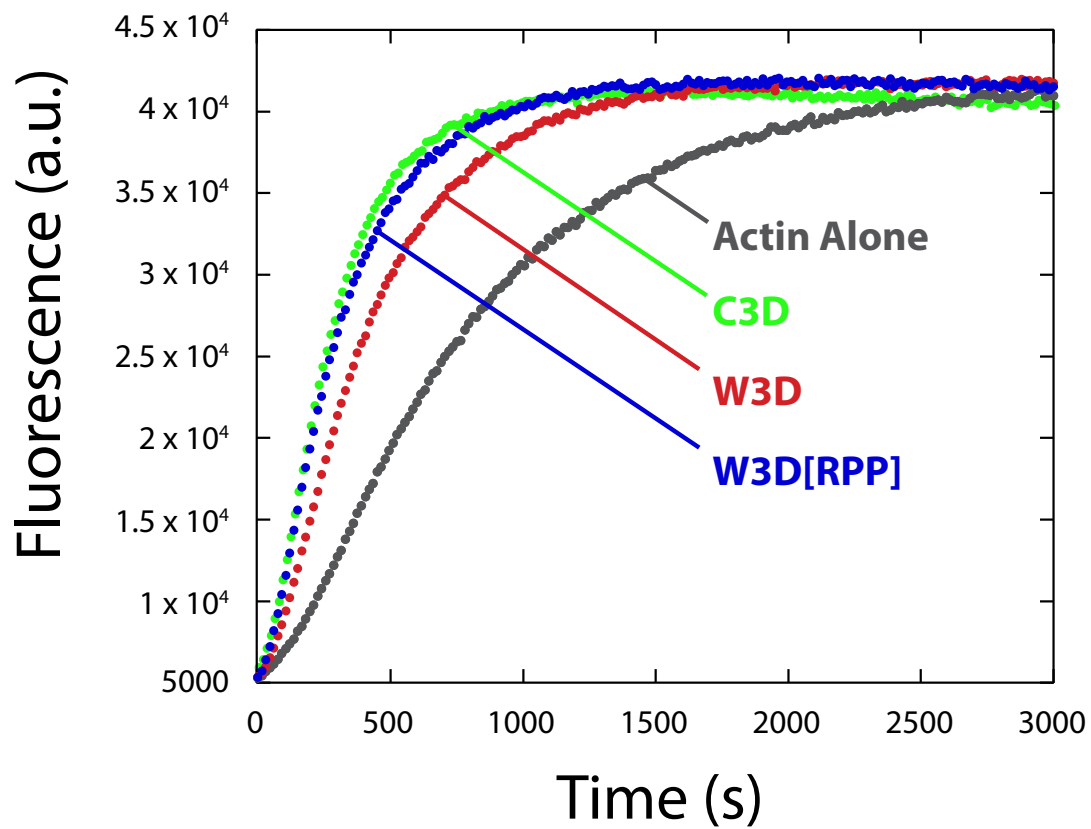


Figure 3.6: Replacing the bridge of W_a with that from WH2C makes a stronger nucleator. Representative traces of actin polymerization in the presence of wild type C3D (green), W3D (red), or mutant W3D[RPP] dark blue. Actin alone is shown in grey.

Date	Screen	Proteins	Temp °C
4.9.2012	1a Emerald Biosystems Wizard I/II	WH2C3/Actin	18
	1b Hampton Research CS I/II	WH2C3/Actin	18
	1c Hampton Research Index	WH2C3/Actin	18
	1d Qiagen JSGC+	WH2C3/Actin	18
	1e Qiagen PACT	WH2C3/Actin	18
4.20.2012	Sodium Citrate Refinement		
	2a (0.1M CHES pH9.5, 0.8-1.275M NaCitrate)	WH2C3/Actin	18
4.27.2012	pH Refinement		
	3a (0.1M CHES pH 8.73-10.01, 0.9104M NaCitrate)	WH2C3/Actin	4
	3b (0.1M CHES pH 8.73-10.01, 0.9104M NaCitrate)	WH2C3/Actin	18
5.01.2012	Hampton Additive Screen		
	4a (0.1M CHES pH 9.5, 0.9104M NaCitrate)	WH2C3/Actin	18
6.04.2012	5a Emerald Biosystems Wizard I/II	C3D/Actin	18
	5b Hampton Research CS I/II	C3D/Actin	18
	5c Qiagen ProComplex	C3D/Actin	18
	5d Qiagen JSGC+	C3D/Actin	18
	5e Qiagen PACT	C3D/Actin	18
6.11.2012	6a Qiagen ProComplex	C3D/Actin	4
	6b Hampton Research CS I/II	C3D/Actin	4
6.14.2012	7a Emerald Biosystems Wizard I/II	C3D/Actin	4
	7b Qiagen JSGC+		
6.15.2012	8a Emerald Biosystems Wizard I/II	WH2C/Actin	18
	8b Hampton Research CS I/II	WH2C/Actin	18
	8c Hampton Research Index	WH2C/Actin	18
	8d Hampton Research SaltRx	WH2C/Actin	18
	8e Qiagen JSGC+	WH2C/Actin	18
	8d Qiagen PACT	WH2C/Actin	18
	8e Qiagen AmSO4	WH2C/Actin	18
7.11.2012	PEG-8000 Refinement		
	9a (0.1M CHES pH 9.5, 0.3%-20% w/v PEG-8000)	WH2C/Actin	18
	9b (0.1M CHES pH 8.8, 0.3%-20% w/v PEG-8000)	WH2C/Actin	18
	Sodium Citrate Refinement		
	9c (0.1M CHES pH9.5, 0.6-1.075M NaCitrate)	WH2C/Actin	18
	9d (0.1M CHES pH8.8, 0.6-1.075M NaCitrate)	WH2C/Actin	18
7.11.2012	Hampton Additive Screen		
	9e (CHES pH9.5, 20% PEG-8000)	WH2C/Actin	18
	9f (CHES pH9.5, 1M NaCitrate)	WH2C/Actin	18
7.17.2012	10a Qiagen ProComplex	WH2C/Actin/Dnase-I	18
7.17.2012	Sodium Citrate Refinement		
	11a (0.1M CHES pH9.5, 0.8-1.275M NaCitrate)	WH2C3/Actin	18
7.17.2012	Vapor Diffusion - Sodium Citrate Refinement		
	12a (0.1M CHES pH9.5, 0.8-1.03M NaCitrate)	WH2C3/Actin	18

Table 3.1: A summary of different crystal conditions describing the screens, temperatures, and constructs used.

Observation

- 1a** Crystals: *F4*
- 1b** Microcrystals: *B10, C12, D6, F6, and F9*
- 2a** Granular: *A1-12*
Precipitate: *B1-5, D1-12, E1-12, F1-3, F5-12, G1-5, G6-12 and H1-12*
Crystals: *C1-12*
Crystals well dispersed: *G6*
Large crystals: *B5-12*
- 3b** Small crystals in wells with pH: *9.82, 9.92, 9.41 and 10.01*
Large granular precipitation in wells with pH: *8.93, 9.23, 9.31, 9.5, and 9.61*
- 4a** Crystals: *A3, A6, and D12*
Small crystals: *B2,B7,B10,B11, and most of row C*
- 8a** Large crystals: *A1 and D10*
Crystals: *F4*
- 8d** Needles: *E3, F3, and G3*
- 9a** Small crystals: *F8, F9,F10, F11, G1, and G2-G8*
- 9b** Gel: *C8, C11, and F3*
Tiny spheres: *F9*
Tiny crystals: *G3*
Medium crystals: *G2*
Large crystals: *G4, G6, G7, G8, and G10.*
- 9c** Crystals at the edge: *C2*
Crystals: *C3, C4, C6, C7, C8, D6, E1, F1, and G1*
- 9d** Small crystals at the edge: *D1 and D10*
Small crystals: *D7*
Branching crystals: *D9*
Large crystals in *E1, E4, E7, F11, F12, and G1*
Crystals: *the rest of the conditions*
- 9f** Tiny crystals: *A1*
Small crystals: *A6*
Larger crystals: *B4*
Polymorphic: *C2, C3, H1, and H6*
Very Large crystals: *C9*
Medium Crystals: *D4, D5, and D8*
Crystals: *E5 and H8*
Crystals at the edge: *F8*
Odd crystals: *G3*
- 11a** Flakey crystals: *A1-A9, B1-B9, C1-C9, D1-D9, E1-E9, F1-9, G1-9, H2-9*
Crystals: *E11-12, F12, G12, and H1*

Diffraction Tests

- G6:** 0.1M CHES pH 9.5, 1.185M NaCitrate
Cryoprotectant: Parafin oil
Collected 2 sets of diffraction at 90°, distance 150
Multiple crystals were looped so data looks like a powder diffraction experiment
- B10:** 0.1M CHES pH 9.5, 0.905M NaCitrate
Cryoprotectant: none
Collected 2 sets of diffraction at 90°, 300s exposure, distance of 150
Observed definite diffraction spots at both angles
- D3:** 0.1M CHES pH 9.5, 0.99M NaCitrate
Cryoprotectant: Parafin oil
Diffraction at 90°, 300s exposure, distance of 150
Observed weak diffraction spots
- B11:** 0.1M CHES pH 9.5, 0.91M NaCitrate
Cryoprotectant: Parafin oil
Diffraction at 360°, 300s exposure, distance of 180
Observed a low-resolution diffraction at 3.7 Å
- 0.1M CHES pH 9.41, 0.91 M NaCitrate**
Cryoprotectant: Parafin oil
Diffraction at 0° and 90°, 300s exposure, and distance of 180
Observed a low-resolution diffraction in both images
- 0.1M CHES pH 9.73, 0.9104M NaCitrate**
Cryoprotectant: None
Diffraction at 0° and 90°, 300s exposure, distance of 180
Observed a shadow of a diffraction
- A6:** 0.1M CHES pH 9.5, 0.91 M NaCitrate, 0.1 M Magnesium chloride hexahydrate
Cryoprotectant: MPD
Diffraction at 90°, 300s exposure, distance of 180
No diffraction
- A6:** 0.1M CHES pH 9.5, 0.91 M NaCitrate, 0.1 M Magnesium chloride hexahydrate
Cryoprotectant: Glycerol
Diffraction at 90°, 300s exposure, distance of 180
No diffraction
- H11:** 0.1M CHES pH 9.5, 0.91 M NaCitrate, 40% v/v 2,2,2-Trifluoroethanol
Cryoprotectant: Parafin oil
Collected 2 sets of diffraction at 90°, 300s exposure, distance of 150
Observed a low-resolution diffraction that was highly anisotropic
- B2:** 0.1M CHES pH 9.5, 0.91 M NaCitrate, 0.1 M Praseodymium(III) acetate hydrate
Cryoprotectant: Parafin oil
Collected 2 sets of diffraction at 90°, 300s exposure, distance of 150
Observed very weak diffraction
- A1 and D10** had weak UV fluorescence
- C4:** 0.1M CHES pH 9.5, 0.735 M NaCitrate
Cryoprotectant: None
Collected 2 sets of diffraction at 90°, 300s exposure, distance of 150
Low-resolution diffraction
- C6:** 0.1M CHES pH 9.5, 0.745 M NaCitrate
Cryoprotectant: Parafin oil
Collected 2 sets of diffraction at 90°, 300s exposure, distance of 150
Observed very weak diffraction
- E4:** 0.1M CHES pH 8.8, 0.855 M NaCitrate
Cryoprotectant: Glycerol
Collected 2 sets of diffraction at 90°, 300s exposure, distance of 150
Observed 4 Å spots

Table 3.2: A summary describing the type of crystals observed from different screens and the results from testing their diffraction. Bold black numbers and letters represent a code shown in Table 3.1 describing the crystal screen used.

References

- [1] Chen, C.K., M.R. Sawaya, M.L. Phillips, E. Reisler, and M.E. Quinlan Multiple forms of Spire-actin complexes and their functional consequences. *J Biol Chem* 2012;287:10684-10692.
- [2] Ducka, A.M., et al. Structures of actin-bound Wiskott-Aldrich syndrome protein homology 2 (WH2) domains of Spire and the implication for filament nucleation. *Proc Natl Acad Sci U S A* 2010;107:11757-11762.
- [3] Chereau, D., F. Kerff, P. Graceffa, Z. Grabarek, K. Langsetmo, and R. Dominguez Actin-bound structures of Wiskott-Aldrich syndrome protein (WASP)-homology domain 2 and the implications for filament assembly. *Proc Natl Acad Sci U S A* 2005;102:16644-16649.
- [4] Rebowski, G., S. Namgoong, M. Boczkowska, P.C. Leavis, J. Navaza, and R. Dominguez Structure of a longitudinal actin dimer assembled by tandem w domains: implications for actin filament nucleation. *J Mol Biol* 2010;403:11-23.
- [5] Aguda, A.H., B. Xue, E. Irobi, T. Preat, and R.C. Robinson The structural basis of actin interaction with multiple WH2/beta-thymosin motif-containing proteins. *Structure* 2006;14:469-476.
- [6] Hertzog, M., et al. The beta-thymosin/WH2 domain; structural basis for the switch from inhibition to promotion of actin assembly. *Cell* 2004;117:611-623.
- [7] Lee, S.H., F. Kerff, D. Chereau, F. Ferron, A. Klug, and R. Dominguez Structural basis for the actin-binding function of missing-in-metastasis. *Structure* 2007;15:145-155.
- [8] Vizcarra, C.L., et al. Structure and function of the interacting domains of Spire and Fmn-family formins. *Proc Natl Acad Sci U S A* 2011;108:11884-11889.
- [9] Didry, D., et al. How a single residue in individual beta-thymosin/WH2 domains controls their functions in actin assembly. *EMBO J* 2012;31:1000-1013.

Chapter 4: Conclusion

We set out to determine how the WH2 domains of Spir contribute to actin nucleation and how each differs from the WH2 domains in non-nucleating proteins. We studied the interactions between actin and various Spir WH2 constructs under both kinetic and steady state conditions, using an array of biochemical assays in combination with physical modeling. Our findings show that all four WH2 domains of Spir are biochemically distinct from one another and in some cases in ways that are undocumented for WH2 domains. We also determined that Spir WH2C is specialized for nucleation, and that when part of a nucleating construct, it can bind actin cooperatively and promote nucleation.

We took a reductionist approach to examining Spir's nucleation activity by studying each individual WH2 domain and their interactions with actin. We found that despite their short and similar sequences, affinities of the four Spir WH2 domains for actin varied by >100-fold, ranging from 90 nM to over 1 μ M. Furthermore, each inhibited spontaneous bulk actin polymerization, nucleation, and elongation phases in ways uncorrelated with their affinity for actin monomers. We found that only WH2A weakly capped elongating actin filaments, determined by watching actin grow from pre-seeded nuclei using Total Internal Reflection Fluorescence microscopy. Capping fits with how WH2 domains bind to actin, within the hydrophobic cleft of monomers, which is at the barbed end of a filament. Binding here would be expected to change the kinetics of a new actin monomer binding to the weakly capped filament. Perhaps it is surprising that the three other Spir WH2 domains do not have an effect on filament elongation. That said, the WH2 domain and actin interaction that stands out the most is WH2C and its ability to bind actin filaments, an interaction undocumented for any known WH2 domain.

In Chapter 1 we made chimeras consisting of Spir WH2 domains and non-nucleating N-Wasp WH2 domains tethered to each other by Spir Linker 3 (L3). We found that the WH2 domain located N-terminal to Linker 3 influenced the nucleation activity the

most. Multiple constructs with N-Wasp W_a in this position had similar activities to one another. Likewise, multiple constructs with Spir WH2C N-terminal to L3 produced the strongest nucleators, with C3D displaying the greatest activity. We were surprised to find that simply reversing the order to D3C caused a loss of all nucleation activity, highlighting the importance of domain order to nucleation activity. In addition, we determined that the strongest nucleator, C3D, bound cooperatively to actin, whereas D3C bound with negative cooperativity and was only able to bind to one actin monomer. This agrees with the inability of D3C to nucleate actin filaments, which further supports domain order importance in nucleation activity. In summary, these results illustrate how the nucleation activity of Spir is ultimately greater than the sum of its parts.

Together, our data indicate that WH2C is a special WH2 domain. Work performed with the chimeras described above showed that the position of WH2C with respect to Linker 3 was important and that WH2C itself created the strongest nucleators. Closer examination of the sequence of WH2C led us to two residues—Phe-438 and Ser-441—that flank the conserved IR motif and are unique to WH2C. When these residues were replaced in the weaker W_a 3D construct, its nucleation activity increased to C3D levels. Additionally, preliminary data show that when the bridge region of W_a , in the context of W_a 3D, is replaced with the bridge found in WH2C, it becomes a better nucleator with activity similar to C3D. This provides further evidence that WH2C is specially designed to contribute to the overall nucleation activity of Spir. We predict that replacing the native hydrophilic residue Gln in W_a with the hydrophobic Phe N-terminal to the conserved IR motif allows for the helix to be buried deeper in actin's hydrophobic cleft. In combination, replacing the native charged residue, Glu, in W_a C-terminal to the conserved IR motif with the small, uncharged Ser helps to avoid steric clashes that may result from the deeper binding proposed above. Similarly, the uncommon PP region in the bridge of WH2C may lead to a distinct interaction with the residues on the surface of

actin compared to other WH2 domains. Combining both the unique bridge residues of WH2C and residues flanking the IR region may lead to an even more drastic change in the overall WH2C/actin structure. These data suggest that WH2C binds to actin differently from other WH2 domains, and motivated our attempts to co-crystallize WH2C with actin.

We also discovered that in addition to binding actin monomers, WH2C has the unique ability to bind filaments. Its affinity for filaments is 2 μM , a physiologically relevant number but an affinity weaker than its affinity for monomers (0.21 μM). This may explain why we are unable to resolve a structure of WH2C bound to actin despite the successful crystallization of other WH2 domains with actin [1-7]. WH2C likely exists in equilibrium between its two binding sites, making it difficult to capture just one of them. When crystalizing C3D and actin, Chen *et al.* solved the structure of WH2D bound to actin, but they were unable to detect WH2C despite the fact that when separate, WH2C binds (monomeric) actin with higher affinity. Our own attempts led to diffraction at a resolution of 3.7 Å, which is not high enough to see side chain details. We are hopeful that we will ultimately overcome this challenge.

Work by Bosch *et al.*, questioned the ability for Spir to nucleate when they found that under saturating actin conditions, Spir and actin formed a sequestration complex and was unable to organize an actin nucleus [8]. Work by Chen *et al.*, clarified that under saturating actin conditions similar to those in Bosch *et al.*, a mix of both nucleating and sequestering complexes exist, implying there is an equilibrium between the two states [8, 9]. The ability of WH2C to bind actin in two ways, that is to bind both actin monomer and filaments may contribute to nucleation activity by allowing Spir to “get out of the way” during filament formation while still remaining loosely associated through the filament affinity. This could be part of the equilibrium Chen *et al.* observed. Similarly, we

envision WH2A weakly capping the actin nucleus, stabilizing a sequestration complex when bound and allowing nucleation when it releases the structure. Together these data support a model where each WH2 domain binds an actin monomer, brings them into close proximity with one another, and then subsequently adjusts without completely dissociating to allow for filament formation (Figure 4.1).

Our findings here help to clarify how Spir nucleates actin filaments, and further how Spir differs from other non-nucleating WH2 containing proteins. We highlight how subtle changes to the sequence of various WH2 domains, despite their short lengths and overall sequence conservation, can determine their roles in nucleation, filament capping, monomer binding, and filament interaction. Furthermore, the detailed biochemical foundation we built contributes to a mechanistic model for the nucleation activity of Spir—however many questions remain unanswered.

Our data suggest that the kinetics of actin binding are different for each of Spir's WH2 domains. Since actin assembly is a dynamic process, detailed kinetic characterization of single and tandem WH2 constructs would provide further insight to the nucleation activity of Spir.

Previous data demonstrates that tandem WH2 constructs tethered by Linker 3 will nucleate actin filaments [10, 11]. Our cooperativity data further refined the requirements that both WH2 domains must be able to bind to one actin monomer. Our reverse D3C construct could not nucleate and could only bind to one actin monomer – we do not know if this monomer bound preferentially to one of the WH2 domains or not. This provides insight into previous data from Quinlan *et al.*, where each WH2 domain in the WH2 cluster of Spir was individually mutated to abolish actin binding [10]. They saw the largest decrease in nucleation activity when WH2D was mutated. We were surprised to find that WH2C was so important in light of these data. After observing our cooperativity data, we predicted that the original WH2D mutated construct had the

weakest nucleation activity because, in this case, two functional WH2 domains did not flank L3. Further, the WH2-nucleator JMY has a linker homologous to Spir L3, and like L3, it can serve to create nucleation activity when placed between two non-nucleating WH2 domains [11]. These data bring into question how Linker 3 contributes to the nucleation activity of Spir and will require a more detailed analysis of its interaction with actin.

Spir has been proposed to be a dimer. Whether or not this is true, it can be dimerized by its interaction with a second protein, Cappuccino. Dimerization enhances Spir's nucleation activity [12, 13]. How it does so is unknown. What does the nucleus of a Spir dimer look like compared to a Spir monomer? Furthermore, how do these nuclei differ from those formed by other known WH2-nucleators? Continuing this work will help us refine our understanding of WH2-nucleation and lead to a more complete mechanistic understanding of the dynamic actin cytoskeleton.

Figure 4.1:

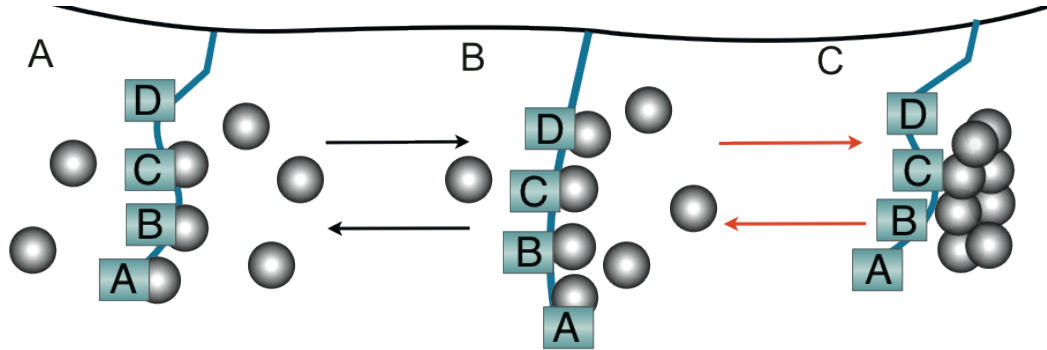


Figure 4.1 A model of Spir nucleation. The WH2 domains of Spir will bind to some number of actin monomers (A) bringing them into close proximity with each other increasing the local concentration of actin (B). Actin monomers can then begin to associate with one another to form a nucleus and dissociate from the WH2 domains while still remaining attached through WH2C's ability to bind filaments (C). The arrows depict an equilibrium between these different states. (B) shows how the capping activity of WH2A may form a stable sequestration complex, which is in equilibrium (red arrow) with the formation of a nucleating complex (C).

Reference

- [1] Chen, C.K., M.R. Sawaya, M.L. Phillips, E. Reisler, and M.E. Quinlan Multiple forms of Spire-actin complexes and their functional consequences. *J Biol Chem* 2012;287:10684-10692.
- [2] Chereau, D., F. Kerff, P. Graceffa, Z. Grabarek, K. Langsetmo, and R. Dominguez Actin-bound structures of Wiskott-Aldrich syndrome protein (WASP)-homology domain 2 and the implications for filament assembly. *Proc Natl Acad Sci U S A* 2005;102:16644-16649.
- [3] Sitar, T., J. Gallinger, and A. Ducka..., *Molecular architecture of the Spire-actin nucleus and its implication for actin filament assembly*, in *Proceedings of the ...* 2011.
- [4] Rebowski, G., S. Namgoong, M. Boczkowska, P.C. Leavis, J. Navaza, and R. Dominguez Structure of a longitudinal actin dimer assembled by tandem w domains: implications for actin filament nucleation. *J Mol Biol* 2010;403:11-23.
- [5] Aguda, A.H., B. Xue, E. Irobi, T. Preat, and R.C. Robinson The structural basis of actin interaction with multiple WH2/beta-thymosin motif-containing proteins. *Structure* 2006;14:469-476.
- [6] Hertzog, M., et al. The beta-thymosin/WH2 domain; structural basis for the switch from inhibition to promotion of actin assembly. *Cell* 2004;117:611-623.
- [7] Lee, S.H., F. Kerff, D. Chereau, F. Ferron, A. Klug, and R. Dominguez Structural basis for the actin-binding function of missing-in-metastasis. *Structure* 2007;15:145-155.
- [8] Bosch, M., K.H.D. Le, B. Bugyi, J.J. Correia, L. Renault, and M.F. Carlier, *Analysis of the function of Spire in actin assembly and its synergy with formin and profilin*, in *Molecular Cell*. 2007. p. 555-568.
- [9] Chen, Z., et al., *Structure and control of the actin regulatory WAVE complex*, in *Nature*. 2010. p. 533-538.
- [10] Quinlan, M.E., J.E. Heuser, E. Kerkhoff, and R.D. Mullins *Drosophila Spire is an actin nucleation factor*. *Nature* 2005;433:382-388.
- [11] Zuchero, J.B., A.S. Coutts, M.E. Quinlan, N.B. La Thangue, and R.D. Mullins, *p53-cofactor JMY is a multifunctional actin nucleation factor*, in *Nature Cell Biology*. 2009. p. 451-459.
- [12] Quinlan, M.E., S. Hilgert, A. Bedrossian, R.D. Mullins, and E. Kerkhoff, *Regulatory interactions between two actin nucleators, Spire and Cappuccino*, in *The Journal of Cell Biology*. 2007. p. 117-128.
- [13] Vizcarra, C.L., et al. Structure and function of the interacting domains of Spire and Fmn-family formins. *Proc Natl Acad Sci U S A* 2011;108:11884-11889.

Appendix: Ct-Spir purification

Introduction

The focus of the appendix diverges from the nucleation mechanism of Spir and toward understanding how the activity of Spir is regulated by its C-terminal half, Ct-Spir.

To date there are no known regulatory mechanisms controlling Spir's nucleation activity. There are preliminary reports of Spir being phosphorylated by the c-JUN N-terminal Kinase, which may be a mechanism by which Spir is regulated but no functional consequence of this modification has been demonstrated. Rosales-Nieves *et al.* proposed that two isoforms of Spir, Spir-PD and Spir-PC regulate each other [1]. Dahlgard and co-workers used these isoforms of Spir, to complement a Spir null fly that does not build an actin mesh [2]. Spir-PD is approximately the N-terminus of full length Spir, whereas Spir-PC is essentially the C-terminus. GFP-Spir-PD complimented the null, leading to actin mesh formation, but GFP-Spir-PC failed to do so. Although GFP-Spir-PD rescued the mesh, it failed to appropriately disassemble the mesh at stage 10b thus leading to female sterility [3]. These data suggest a regulatory role for the C-terminus of Spir. As further evidence, expression of GFP tagged, full length Spir led to actin mesh formation and the proper onset of streaming in the null fly, leading to the production fertile flies [3].

Additional data suggest that Ct-Spir can bind to the KIND domain in the N-terminal half of Spir (unpublished). This interaction may be a common form of regulation, called autoinhibition, where an intramolecular interaction occurs between the N- and C-termini of a protein that inhibits its own activity. Unfortunately, investigating the regulation of Spir by Ct-Spir has proven very difficult because the purification of Ct-Spir is difficult—only one group has previously reported purifying Ct-Spir [1]. We achieved minimal success after modifying expression methods and purification conditions using a variety of constructs, protein tags, expression systems, and bacterial strains. Preliminary co-expression data did support the interaction previously seen between Ct-Spir and the

KIND domain.

Results

Denature and Renature

A common problem encountered when using *E. Coli* for recombinant protein expression is the sequestration of the expressed protein into insoluble aggregates called inclusion bodies [4]. This is one of the challenges we faced when trying to purify Ct-Spir (Figure A.1 A). Generally elaborate solubilization, refolding, and purification procedures are required to recover functional protein from inclusion bodies. We were able to solubilize Ct-Spir using 8 M urea as a denaturing agent. We then purified it from solution using either Ni-NTA or Co-NTA (“Talon resin”) purifications (Figure A.1 B). We tried to refold Ct-Spir by slowly removing urea from solution either by dialysis or other buffer exchange methods (Figure A.1 C,D). In both cases we exposed the protein solutions to buffers with decreasing concentrations of urea, starting with 8 M and ending at 0 M. Through dialysis we were able to expose Ct-Spir to as little as 0.12 M urea before it would crash out of solution (Figure A.1 C). We had better luck using a buffer exchanging method where Ct-Spir was still bound to resin and subsequently eluted, which yielded some apparently refolded protein (Figure A.1 D). We suspect this technique worked better because Ct-Spir is tethered to the resin and separated from each other, thereby preventing aggregation as they refolded. Although we had some success in denaturing and renaturing Ct-Spir, our yields were low and there are always risks involved when using refolded proteins, that is, even when soluble they may not be correctly refolded and therefore are not functional.

Expression Conditions

We next tried to optimize our expression conditions to increase the solubility of Ct-Spir without using denaturant. Since we know over expression of recombinant proteins triggers the formation of inclusion bodies, we induced various amounts of

protein expression over different times. To alter the amount of protein expressed, we reduced the concentration of induction agent, isopropyl β -D-1-thiogalactopyranoside (IPTG), when inducing protein expression. The concentration of IPTG we added ranged from 50 μ M to 250 μ M. In order to further fine tune the level of protein expression, we also altered the length of time allowed for induction from 1 h to 20 h. To analyze the different expression conditions, we lysed cells from each condition and analyzed the levels of induced protein expression by PAGE (Figure A.2 A-E). Unfortunately, we saw little to no change under the different conditions. Additionally, we altered the type of growth media and temperature during induction, but these changes also led to no increase in soluble protein production. Since we were unsuccessful in increasing the amount of soluble Ct-Spir by altering the expression conditions, we next decided to alter the lysis buffer used to possibly dissolve the insoluble protein. We varied the pH, in addition to changing the concentrations of salts and detergents (Figure A.3). We again saw no changes in the concentration of soluble Ct-Spir.

Purification Conditions

Rosales-Nieves *et al.* reported the successful expression and purification of multiple C-terminal Spir constructs [1]. After obtaining the DNA from them for two C-terminal constructs they refer to as SpirC3A and SpirC3, we expressed and purified them using a protocol similar to the one described in Chapter 1 in parallel with the purification method used by Rosales-Nieves and co-workers [1]. Expression tests revealed strong expression of SpirC3A but not SpirC3, so we focused our efforts on getting SpirC3A purified to homogeneity (Figure A.4 A). Both purification protocols yielded GST-tagged SpirC3A; the protocol from Chapter 1 yielded ~2 fold more protein

than that used by Rosales-Nieves and co-workers (Figure A.4 B, C) [1]. Unfortunately after GST cleavage, both SpirC3A elutions degraded.

In further attempts to obtain pure protein, we altered a number of other purification elements including construct size, purification tag identity, expression system, and the addition of various metal ions. We created a number of different constructs using different tags to try and stabilize the Spir fragment (Figure A.5). We expressed these constructs in the bacterial strains BL21, Rosetta, EXP-RV1337-5, and Arctic Express, as well as the baculovirus expression systems using SF9 insect cells. We were able to purify large quantities of Spir constructs using the Arctic Express competent cell but we could not separate it from the tightly bound strain-specific stabilizing chaperones despite numerous ATP washes performed. Lastly, the C-terminus of Spir contains a modified FYVE domain, which is thought to require cation coordination for proper folding. We included either zinc or cadmium ions during all steps of expression and purification, but unfortunately we did not see any appreciable gains in Spir yield.

Functional Assays

Preliminary co-immunoprecipitation results have shown that Ct-Spir can bind the KIND domain of Spir. We co-expressed GST tagged Ct-Spir and His-tagged KIND in an attempt to stabilize Ct-Spir for successful purification. After eluting from glutathione resin, we detected both Ct-Spir and the KIND domain by Western blot, which indicated that a stable interaction occurs between the two (Figure A.6 A,B). This observation allowed me to use this interaction as a functional assay to determine if the Ct-Spir constructs we purified properly.

We first performed pull down assays using purified Ct-Spir that was expressed in *E. Coli* BL21 competent cells and purified using a denaturation and subsequent

renaturation method. The next pull downs we performed used lysate from either SF9 cells or Arctic Express cells expressing Ct-Spir and purified KIND domain. All three pull down experiments gave inconclusive results (Figure A.7 A,B,C). Both Ct-Spir and KIND are present in bound and unbound fractions. Even when we swapped the construct that was pulled down, we still saw the same result.

In order to examine the regulatory mechanism used by Spir, we used many techniques to express and purify its C-terminal half. We had some success in purification, but further refinement is needed in order to develop an efficient and cost effective method for purification of functional Ct-Spir.

Methods

GST pull-down Assay

All steps were performed in 250 mM NaCl, 25 mM HEPES, pH 7.0, 5 mM MgCl₂, 25 μM ZnSO₄, and 1mM DTT. 0.22mg of purified GST or 6xHis tagged Spir KIND domain with either GST or 6xHis tagged Spir over-expressed cell lysate or purified Spir constructs were mixed with 75uL of GST slurry for 1 h. Samples of supernatant were taken after centrifugation as the unbound sample. Resin was washed 3 x 100 μL buffer before SDS-Page protein loading dye was added and used as the bound sample. Samples were analyzed by SDS-Page or Western blotted against GST and 6xHis.

Protein Purifications

We used variations of the purification methods described in Chapter 1 using GST, TALON, and Ni²⁺ resin. In cases where Spir was denatured, we rocked the lysed cell pellet in buffers containing 8 M Urea overnight at 25 °C.

Baculovirus Expression

All Spir constructs were subcloned into baculovirus expression vectors containing either an N-terminal GST or a C-terminal 6xHis tag. The recombinant baculovirus was generated using the Bac-to-Bac baculovirus expression system (Invitrogen 10359-016). Exponentially growing SF9 cells at 2×10^6 cells/ml were infected with $\sim 1 \times 10^6$ P2 virus of each component per 1 L of culture. The culture was incubated, shaking at 90 rpm and 27 °C. Cells were harvested at ~ 96 h post infection. Purification is similar to that described in Chapter 1 with the modification that the lysis buffer was supplemented with complete protease inhibitors (Roche).

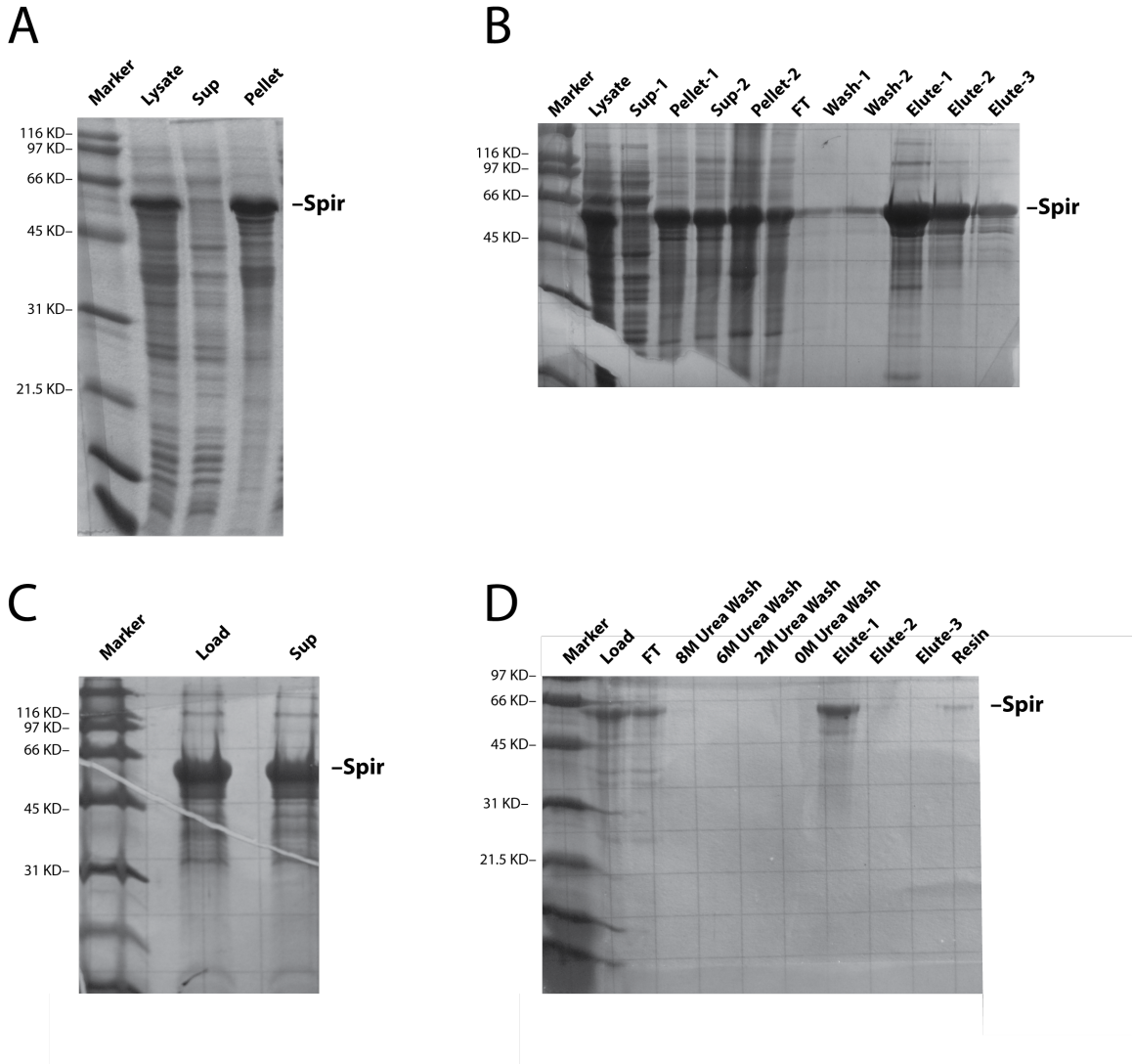


Figure A.1: Ct-Spir in inclusion bodies require denaturing methods for purification. (A) Ct-Spir 520-991 is found in the pellet after centrifugation of the Ct-Spir cell lysate. (B) Isolation of Ct-Spir 520-991 was achieved after it was denatured in 8 M urea and then purified using Talon resin. (C) Ct-Spir 520-991 was successfully introduced into 0.12 M urea through dialyses methods shown by the soluble Ct-Spir fraction. (D) Ct-Spir 520-991 was introduced to 0 M urea conditions before being eluted from Talon resin. Molecular weight markers are labeled to the left of the Coomassie stained PAGE gels.

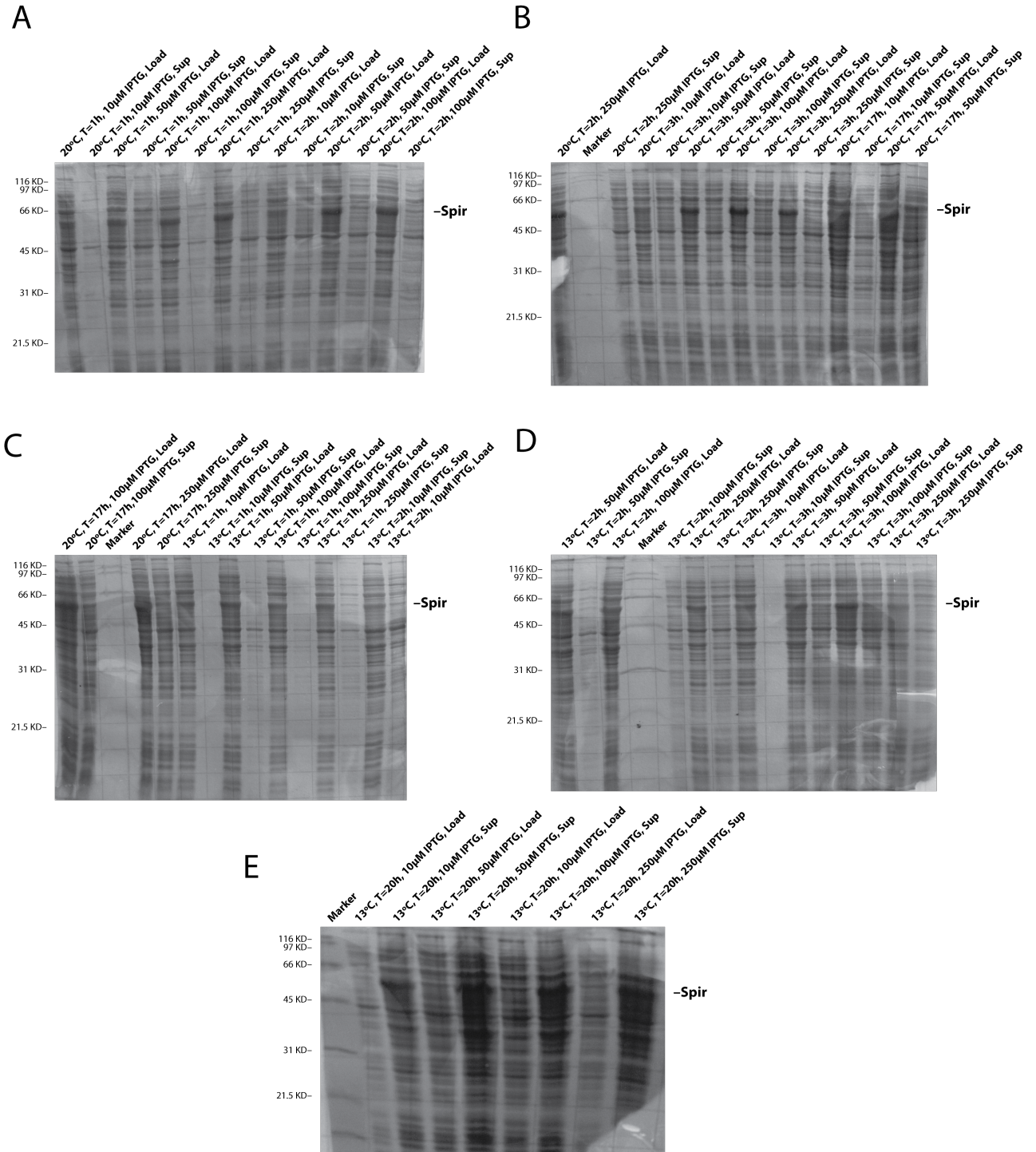


Figure A.2: No increased soluble Ct-Spir was detected from altered expression conditions. (A-E) Ct-Spir 520-991 was expressed in BL21 *E. Coli* competent cells with varying IPTG concentrations, induction time, and temperature. Molecular weight markers are labeled to the left of the Coomassie stained PAGE gels.

	0.1 M KCl	0.2 M KCl	0.2 M KCl
0.02 M Tris, pH 8.0	0.1% NP-40	0.1% NP-40	0.1% NP-40
0.02 M Tris, pH 8.0	0.5% Triton X-100	0.5% Triton X-100	0.5% Triton X-100
0.02 M Tris, pH 8.0	2.0% CHAPS	2.0% CHAPS	2.0% CHAPS
0.02 M Tris, pH 9.0	0.1% NP-40	0.1% NP-40	0.1% NP-40
0.02 M Tris, pH 9.0	0.5% Triton X-100	0.5% Triton X-100	0.5% Triton X-100
0.02 M Tris, pH 9.0	2.0% CHAPS	2.0% CHAPS	2.0% CHAPS
0.02 M CAPS, pH 10.0	0.1% NP-40	0.1% NP-40	0.1% NP-40
0.02 M CAPS, pH 10.0	0.5% Triton X-100	0.5% Triton X-100	0.5% Triton X-100
0.02 M CAPS, pH 10.0	2.0% CHAPS	2.0% CHAPS	2.0% CHAPS

Figure A.3: Ct-Spir 520-991 expressed in BL21 *E. Coli* competent cells was lysed in the buffers above varying varying pH, concentrations of salts and detergents.

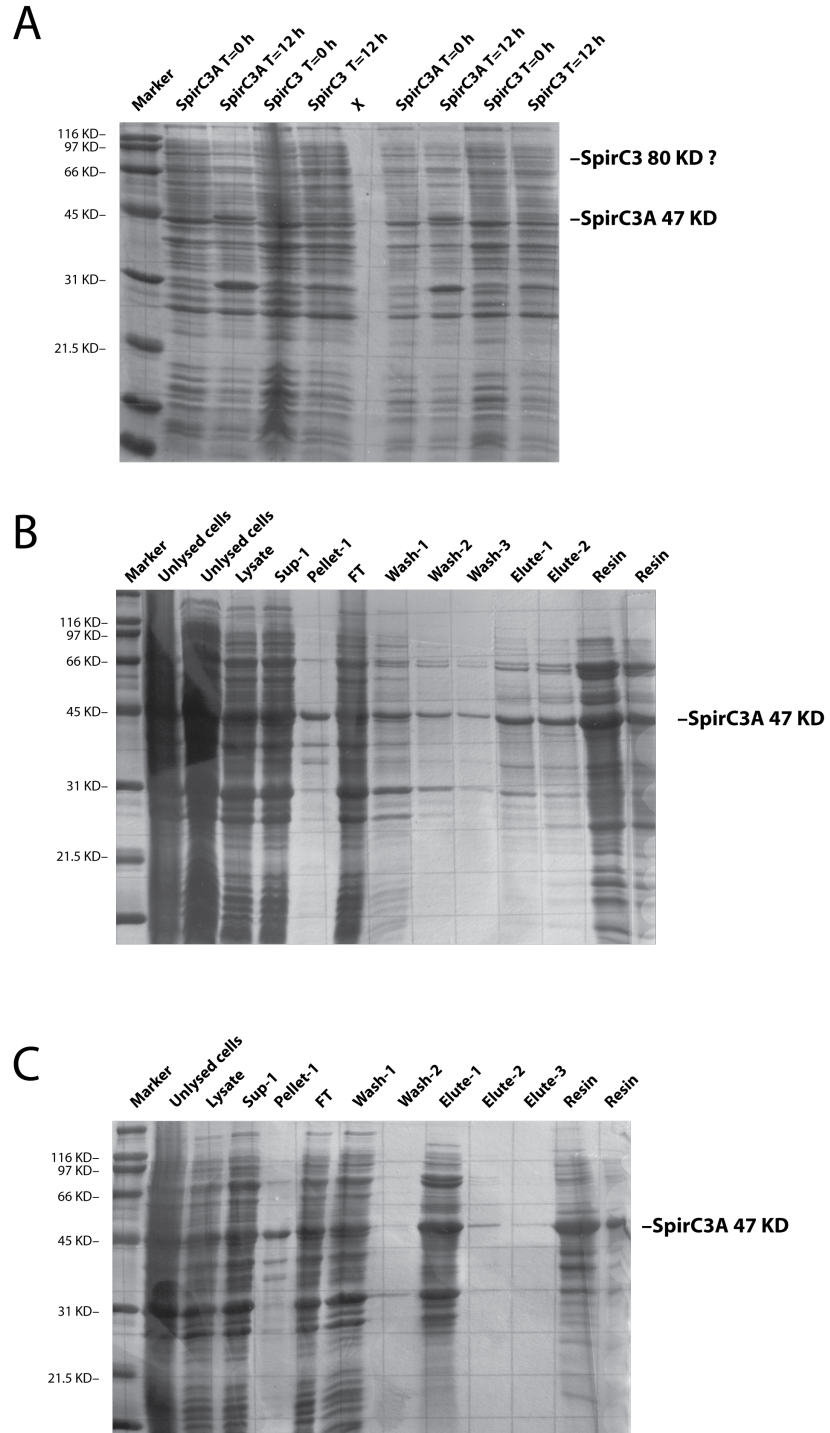


Figure A.4: SpirC3A purification using two different methods. (A) Method as described in Rosales-Nieves *et al.* [1] (B) Method described in Chapter 1. Molecular weight markers are labeled to the left of the Coomassie stained PAGE gels.

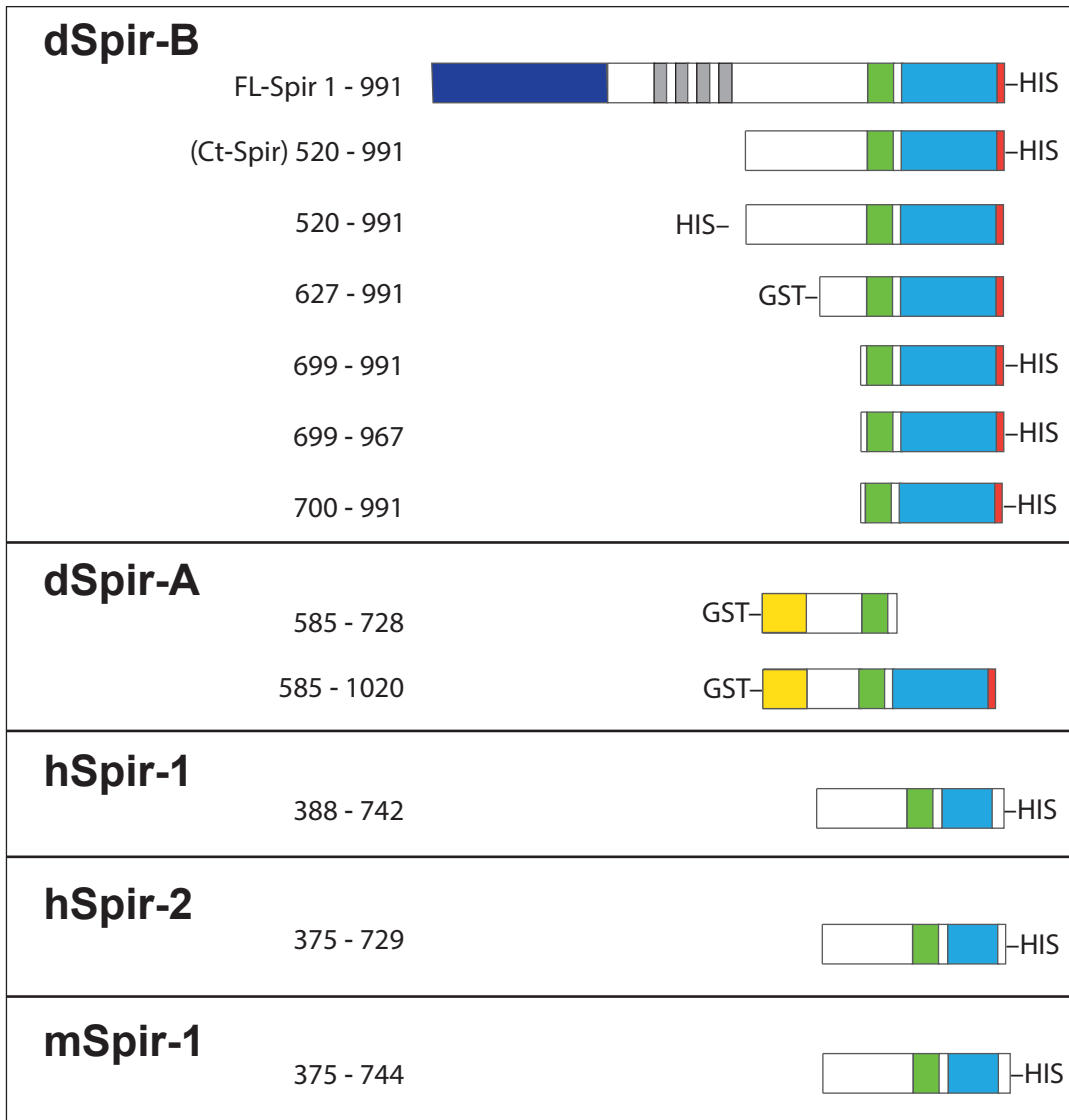


Figure A.5: A schematic showing the different constructs used for purification. Dark Blue-KIND, Grey-WH2 domain, Green-Spir Box, Light Blue-mFYVE, Orange-JNK binding site. Spir isoform and residue numbers for each construct are included.

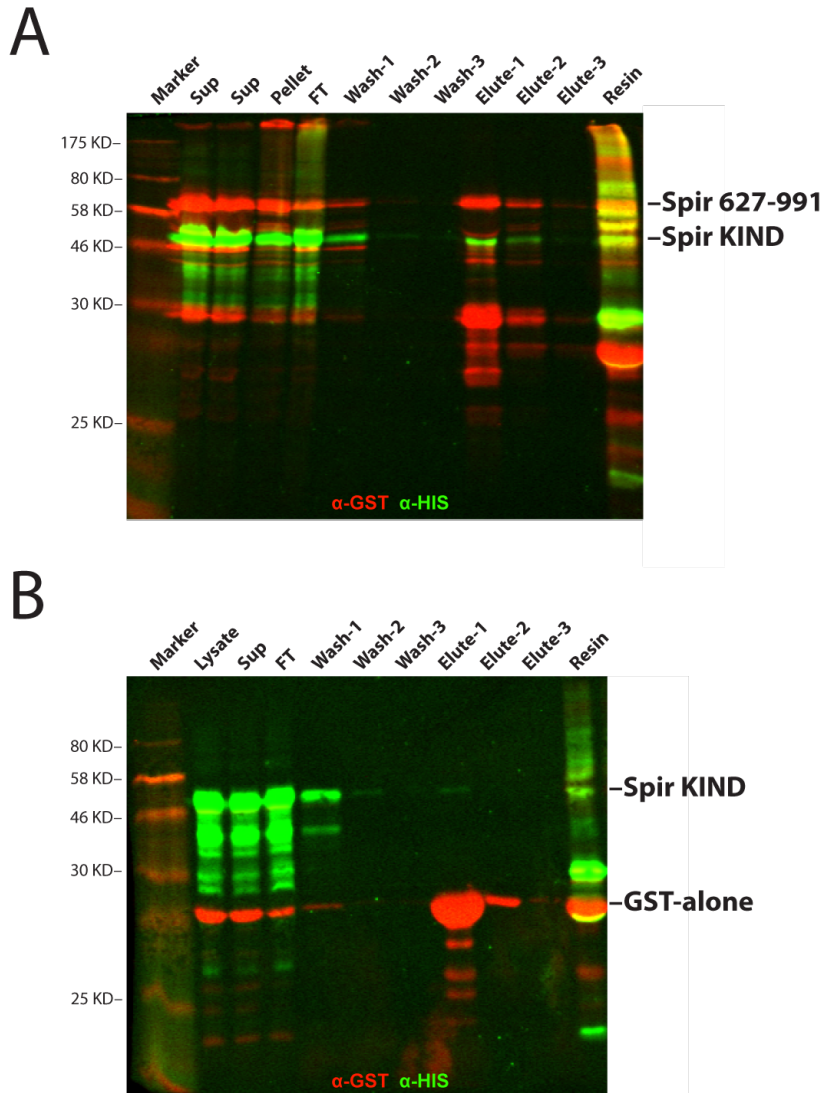


Figure A.6: Co-Purification of Spir 627-991 and KIND. (A) BL21 cells co-expressing GST-tagged Spir 627-991 and His-tagged KIND were purified using glutathione resin. Western blot was performed on samples collected during the purification. Both Spir 627-991 and KIND are detected in the elution fractions. (B) Cells expressing GST-alone and KIND serve as a control showing the specificity of the KIND and Spir 627-991 interaction. No KIND is detected in the elution fractions when co-expressed with GST-alone. Green-anti-GST antibody, Red-anti-His antibody. Molecular weight markers are labeled to the left of the Western blots.

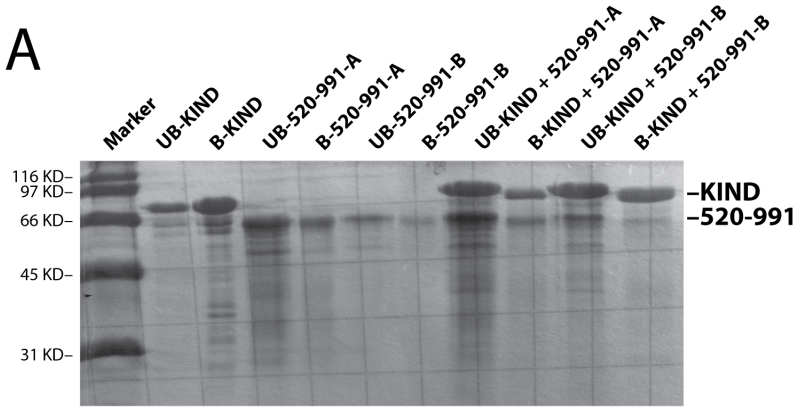
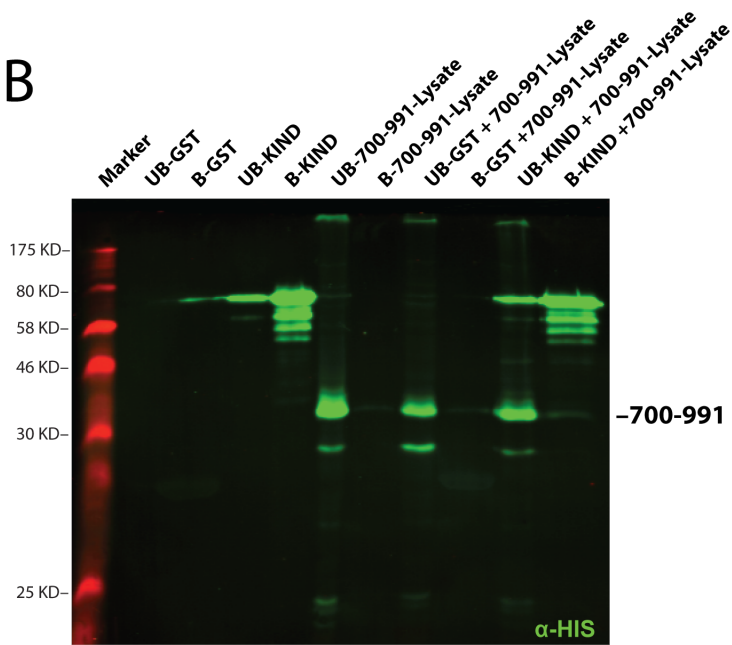
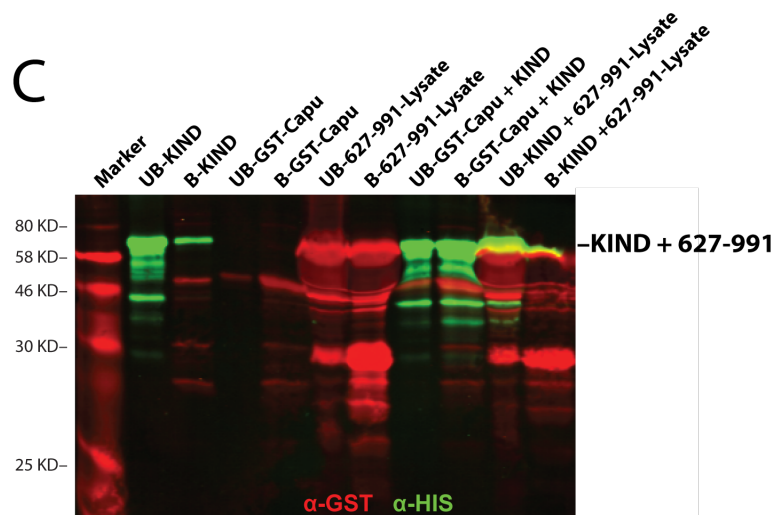
A**B****C**

Figure A.7: Pull-down data with Spir and KIND are inconclusive. (A) Purified His-tagged Ct-Spir 520-991 fractions from Figure A.1,D and purified GST-tagged KIND are mixed together with glutathione resin. Bound and unbound fractions are collected and analyzed by PAGE. (B) His-tagged Spir 700-991 from SF9 cell lysate and purified GST-KIND are mixed together with GST resin. Bound and unbound fractions are collected and analyzed by Western blot. (C) Lysate from Arctic Express cells expressing GST-tagged Spir 627-991 and purified His-tagged KIND are mixed together with glutathione resin. Bound and unbound fractions are collected and analyzed by Western blot. Red-anti-GST antibody, Green-anti-His antibody. In all cases Spir and KIND constructs were both present in bound and unbound fractions when mixed together.

References

- [1] Rosales-Nieves, A.E., J.E. Johndrow, L.C. Keller, C.R. Magie, D.M. Pinto-Santini, and S.M. Parkhurst Coordination of microtubule and microfilament dynamics by *Drosophila* Rho1, Spire and Cappuccino. *Nat Cell Biol* 2006;8:367-376.
- [2] Dahlgaard, K., A.A. Raposo, T. Niccoli, and D. St Johnston Capu and Spire assemble a cytoplasmic actin mesh that maintains microtubule organization in the *Drosophila* oocyte. *Dev Cell* 2007;13:539-553.
- [3] Quinlan, M.E. Direct interaction between two actin nucleators is required in *Drosophila* oogenesis. *Development* 2013;140:4417-4425.
- [4] Kane JF, H.D. Formation of recombinant protein inclusion bodies in *Escherichia coli*. *Trends Biotechnol* 1988;6:95-101.